Petrography and geochemistry of Pharaonic sandstone monuments in Tall San Al Hagr, Al Sharqiya Governorate, Egypt: implications for provenance and tectonic setting

Samir Mahmoud ZAID*, Oussama ELBADRY, Fatma RAMADAN, Mahmoud MOHAMED
Department of Geology, Faculty of Sciences, Zagazig University, Zagazig, Egypt

Abstract: Petrographic and major and trace element compositions of Tanis sandstones from Tall San Al Hagr, Al Sharqiya Governorate, Egypt, have been investigated to determine their source, provenance, intensity of paleoweathering of the source rocks, and tectonic setting. Tanis sandstones are yellowish brown in color, siliceous, partly calcareous, and originated from sands deposited in fluvial channels. Texturally, Tanis sandstones are medium- to very coarse-grained, mature, and moderately sorted. Scarcity of feldspars indicates that the sandstone is extensively recycled from a distant source. Their average modal composition ($Q_{99.75}F_{0.03}L_{0.22}$) classifies them as quartz arenites (quartzite), which is consistent with the geochemical study. Chemical analyses revealed that sandstones have high SiO_2 and $Fe_2O_3^t$ and low Al_2O_3 and TiO_2 values, which are consistent with the modal data. Sandstone samples are enriched in most trace elements such as Zr and Ba, and they are depleted in V, Pb, Sc, Rb, U, and Th. The petrography and geochemistry results suggest that Tanis sandstones were deposited in an intracratonic basin or a passive continental margin of a synrift basin. They were mainly derived from deeply weathered granitic-gneissic sources, supplemented by recycled sands from an associated platform. The CIA and CIW values (60.2 and 87.74, respectively) of the Tanis sandstones indicate moderate to intensive weathering either of the original source or during transport before deposition, and may reflect low-relief and warm humid climatic conditions in the source area. The heavy-mineral and trace element results reveal that the Gebel Ahmar quarry is the probable source for the Tanis sandstones.

Key words: Provenance, Pharaonic sandstone, Tanis, Egypt

1. Introduction

Provenance analysis serves to reconstruct the predepositional history of sedimentary rocks. This includes the distance, climate, and relief in the source area, and the specific type of sedimentary rocks (Pettijohn et al., 1987). Many attempts have been made to refine provenance models using the source rock composition, the extent of weathering, transportation, and diagenesis (Suttner et al., 1981; Bhatia 1983; Dickinson et al., 1983; Taylor and McLennan, 1985; Bhatia and Crook, 1986; Roser and Korsch, 1986, 1988; Suttner and Dutta, 1986; Pettijohn et al., 1987; Kroonenberg, 1994; Weltje et al., 1998; Armstrong-Altrin et al., 2004; Zaid, 2012, 2013). However, the tectonic setting of the sedimentary basin may play a predominant part over other factors, because different tectonic settings can provide different kinds of detritus with variable chemical signatures (Bhatia, 1983; Bhatia and Crook, 1986). For example, the sediments in the passive continental margin tend to have more stable features (rich in SiO_2, low in MgO and Fe_2O_3, etc.), whereas

the sediments in the back arc basin are always rich in mafic rather than felsic rock types (Bhatia and Crook, 1986).

Culturally and historically, Egypt is one of the richest countries in the world. Its precious culture heritage is one of the major attractions for tourism, which represents one of the most important sources of national income. The present study deals with the Pharaonic sandstones in an archaeological site of Tall San Al Hagr (Tanis) in Markz Al-Husayniyyah, Al Sharqiya Governorate (Figure 1). Tanis was an important trading and political center in Pharaonic times and then seems to have declined in importance in the Roman period (Beitak, 1975). The sandstone used to construct the monuments in Tanis is technically known as 'siliceous sandstone', 'silicified sandstone', or 'orthoquartzite', but Egyptologists have long referred to it simply as 'quartzite' (Klemm and Klemm, 2001). However, the geological term 'quartzite' usually refers to a metamorphic rock, whereas in this case it is applied to one that is of sedimentary region. Quartzite, for its durability, was widely used by the ancient Egyptians for small to colossal statuary, sarcophagi, naoi (shrines),
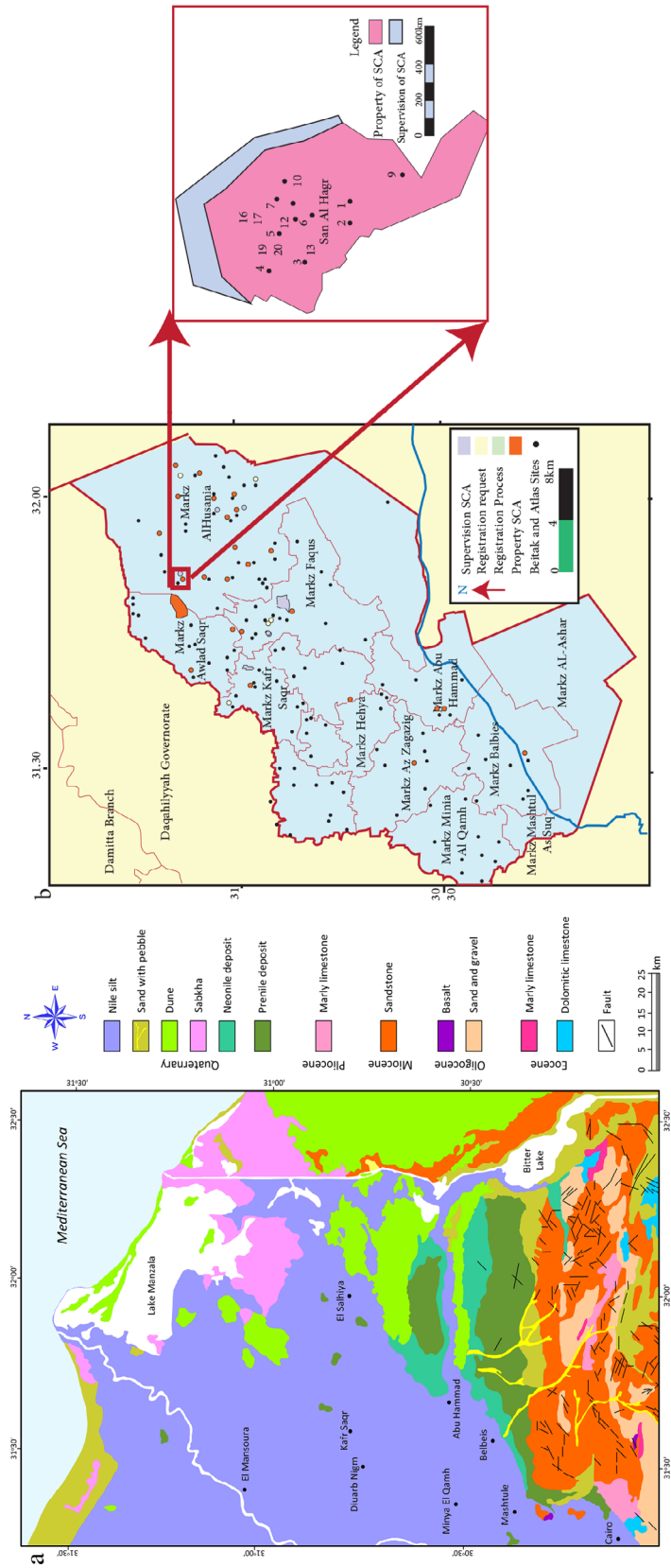
Figure 1. (a) Geologic map and **(b)** location map of Tall San Al Hagr showing the sample locations (modified after, Zaid, 2006).

offering tables, stelae, architectural elements (especially door frames and internal tomb linings), and occasionally barque shrines and obelisks.

The source of the Pharaonic quartzite blocks has long been the subject of discussion, as summarized by Varille (1933), Heizer et al., (1973), Stadelmann (1984), Klemm et al., (1984) and Knox et al. (2009). Although earlier authors reported the occurrence of quartzite at several localities along the Nile Valley (Heizer et al., 1973), it is now clear that true quartzite is restricted to Gebel Ahmar, near Cairo, and the Aswan area (Harrell, 2002; Harrell and Madbouly, 2006; Figure 2). At Aswan, quartzite was extracted from the quarry complex at Gebel Gulab and Gebel Tingar on the west bank of the Nile (Heldal et al., 2005) and from quarries near Wadi Abu Aggag on the east bank (Harrell and Madbouly, 2006).

Early discussion on the source of the quartzite monuments focused on the interpretation of Pharaonic inscriptions and on the logistics of transporting such large blocks from distant quarry sources. Studies on the geology and geochemistry of the quartzites have led to diverging opinions on their provenance. However, geological investigations initially focused on the possibility of distinguishing between the Cairo and Aswan quartzites on the basis of their physical and petrological characteristics. This approach seemed promising in view of the marked difference in age between the two deposits, with the Cairo quartzites being of mid-Tertiary age (Oligocene, ca. 30 Ma) and the Aswan quartzites of Late Cretaceous age (Turonian, ca. 90 Ma) (Hermina et al., 1989; Tawadros, 2001). However, field examination, grain size analysis, and thin-section analysis failed to identify reliable distinguishing features. Both quartzites originated as sands deposited in fluvial channels and display a similar range of bed-forms. Regarding the petrographic properties of the Pharaonic quartzites, previous studies were mainly concerned with the mineralogical and geochemical composition of sandstones (e.g., Abdel Hady, 1988, 2000; Martinet, 1992; Klemm and Klemm, 1993; Knox et al., 2009). No detailed studies on the geochemistry and tectonic setting have been documented. The present work aims to identify the source of the Pharaonic quartzites of the Tall San Al Hagr (Tanis) site. It also aims to identify their tectonic provenance and the paleoweathering conditions of the source area using an integrated approach involving modal analysis and bulk rock geochemistry of the Pharaonic sandstone monuments in Tanis.

2. Geological setting
The study area, Tall San Al Hagr (Figure 1), is located in Sharqiya Governorate (30°58'N, 31°53'E), north Nile Delta, Egypt. The site consists of a large tell that covers a triangular shaped area of about 170 ha. The site covers a distance of 3 km from north to south and 1.5 km at its widest point east to west. The highest point of the tall (in the area known as Gharib San) lies in the northern section of the site and reaches 32 m above sea level.

During the Old and Middle Kingdoms the area was known as the 'Field of Dja'u'. Petrie suggested that the city itself was founded in the XIth or XIIth dynasties, but the first evidence that refers to ancient Tanis is in a Memphite temple dated to the reign of Ramesses II (XIXth Dynasty). Ramesside blocks and sculptures brought here from Tall ad-Dab'ah for use in new buildings led the first excavators of Tanis to erroneously believe that they were really at the Biblical city of Ramesses; it was also formerly erroneously identified with the Hyksos capital of Avaris (EAIS, 2005).

During the Paleozoic and Mesozoic eras of the Phanerozoic Eon, Egypt was alternately elevated above sea level and inundated by shallow seas with mostly siliciclastic sedimentary rocks (conglomerate, sandstone, and mud rock) and limestone. The thickest deposit is the Nubia Group (or Sandstone), which dates to the latter part of the Cretaceous period and was deposited in shallow marine to mainly fluvial environments (e.g., Aswan quartzite at Gebel Gulab, Gebel Tingar, and Wadi Abu Aggag). From the Late Cretaceous through the Eocene epoch of the Tertiary period, the most part of Egypt was under a shallow sea and accumulating carbonate sediments that are best represented today by Eocene limestone formations.

Beginning in the Oligocene epoch and continuing through the Quaternary period, the most part of Egypt was above sea level and once again received predominantly siliciclastic sediments. The mid-Tertiary uplift of Egypt, which initiated the return of siliciclastic sedimentation (e.g., Gebel Ahmar), was caused by the opening of the Red Sea, a plate tectonic rifting event that separated the Arabian Peninsula from the African landmass, beginning about 30 Ma. As a consequence of this rifting, the crystalline basement complex was pushed up to form the Red Sea Hills, a south-to-north flowing paleo-Nile river developed along a fracture zone west of the Red Sea Hills, magmatic activity produced dolerite dikes that intruded all earlier rocks, and volcanic eruptions extruded basaltic lava flows (Said, 1990).

3. Samples and methodology
Twenty fresh samples were collected from Pharaonic sandstone monuments in Tanis (Figure 3). Grain-size analysis was carried out in a Ro-Tap sieve shaker using American Society for Testing and Material (ASTM) sieves ranging from 1.5 f to 4.25 f at 0.50 f intervals for 20 min (Folk, 1966). Heavy minerals were separated using bromoform (sp. gr. 2.85) and the compositions of different heavy minerals were counted and estimated by a binocular microscope (Table 1). Modal mineralogical determinations
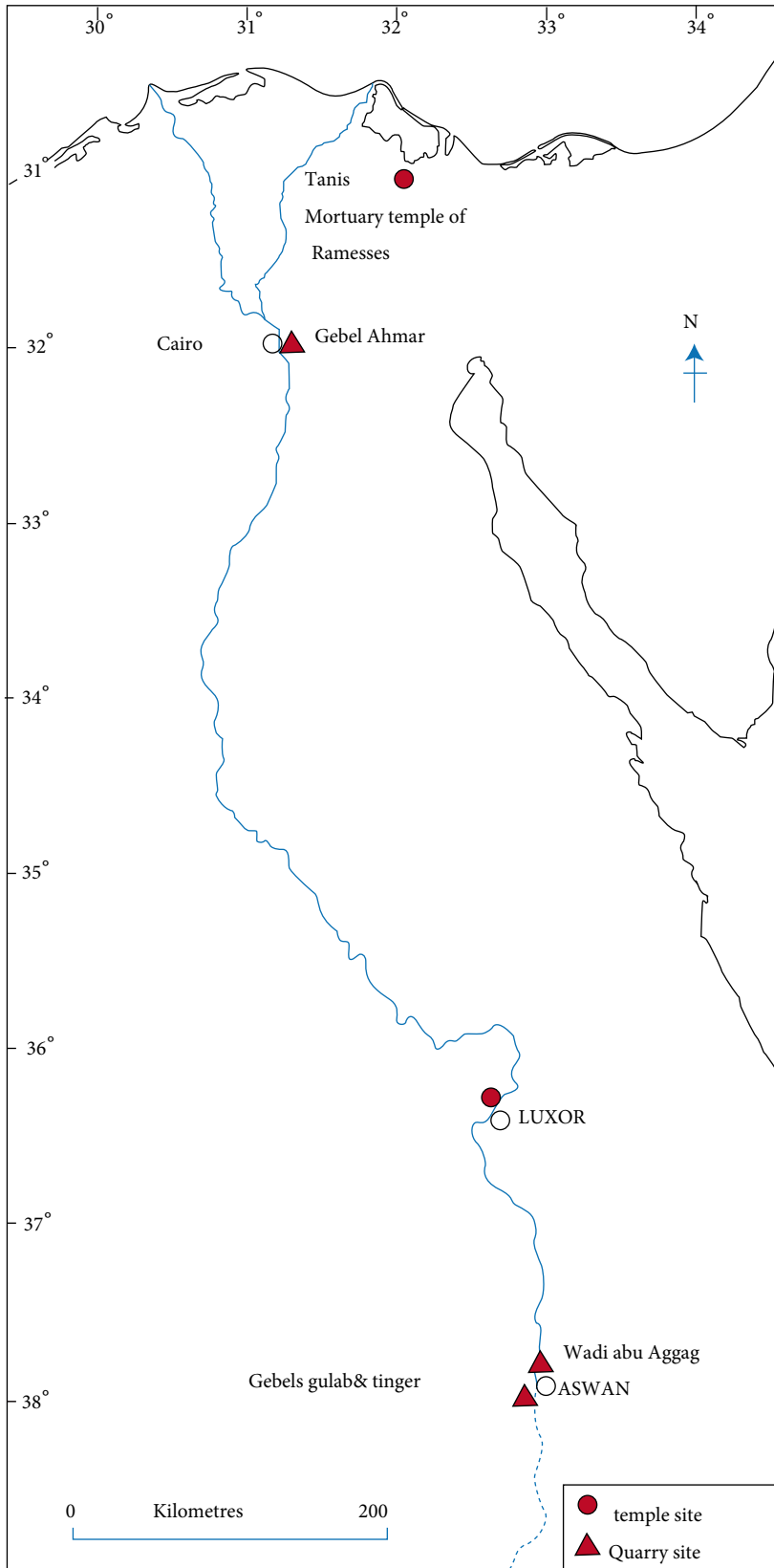
Figure 2. Location map of the Pharaonic sandstone (Tanis) block and other quarries used for comparison.
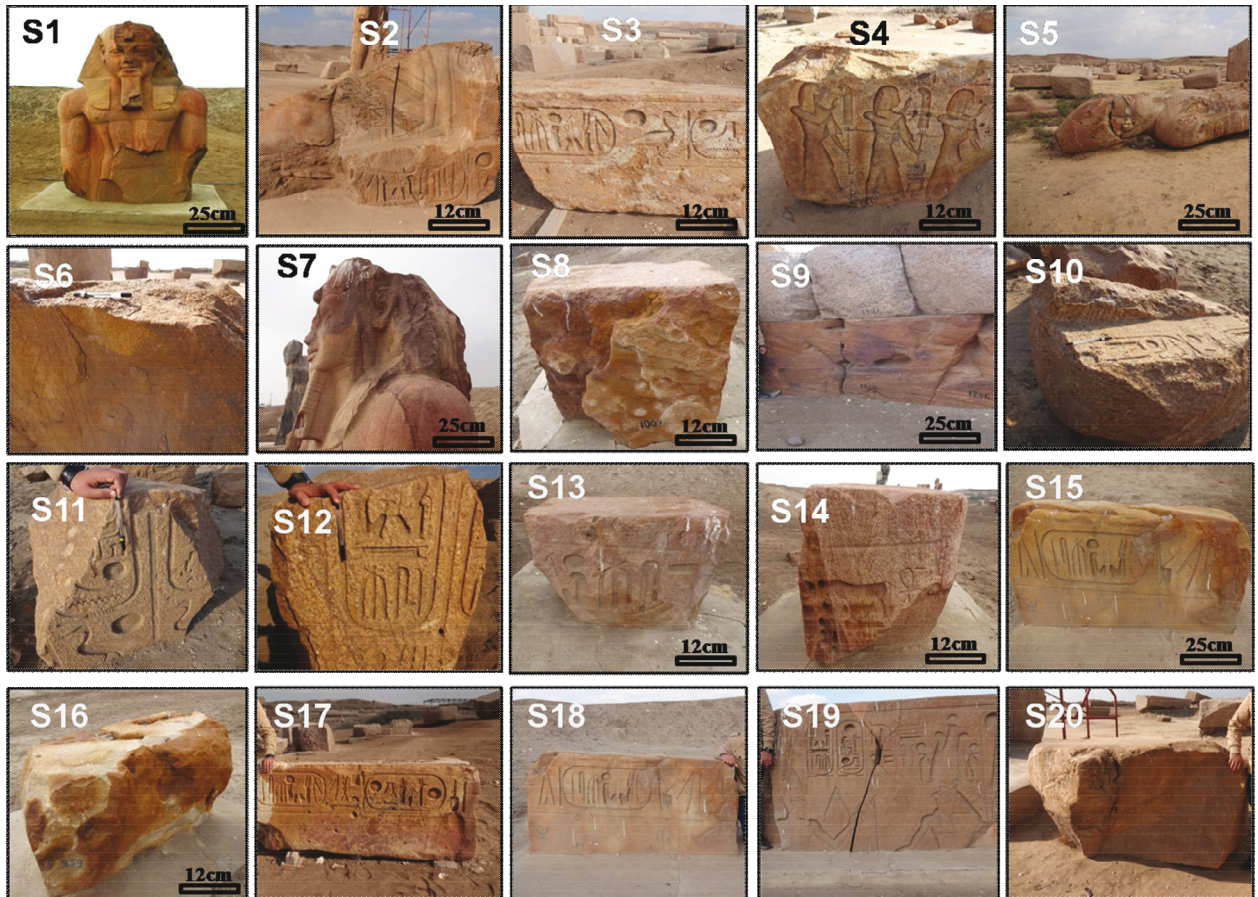
Figure 3. The Pharaonic sandstone monuments in Tall San Al Hagr (Tanis), where the studied samples were collected.

were carried out by counting 300 grains per thin section. The point counts were done usinFg both Gazzi–Dickinson (Gazzi, 1966; Dickinson, 1970) and standard methods to minimize the dependence of rock composition on grain size (Ingersoll et al., 1984). Framework parameters (Ingersoll and Suczek, 1979) and detrital modes of studied sandstone samples are given in Table 2.

The morphology and the textural relationships among minerals were examined in 8 gold-coated samples with a scanning electron microscope (SEM) equipped with an energy-dispersive spectrometer (EDS), using an accelerating voltage of 10 kV. In order to identify the mineralogical composition of sandstones, X-ray diffraction (XRD) analyses of the <2 μm fraction were performed with a Philips PW 1729 diffractometer for 8 oriented samples. The samples were air-dried, ethylene glycol-saturated, and heated at 550 °C for 2h.

X-ray fluorescence spectrometer (XRF), XRD, and SEM-EDS analyses were performed at the laboratories of the National Research Center and Nuclear Materials Authority of Egypt. All 20 samples (fine-grained sands) were analyzed for major and trace element geochemistry.

The major and trace element concentrations were determined in 20 bulk samples using XRF. Analytical precision was better than 5% for the major oxides and trace elements. Loss of ignition (LOI) was estimated by heating the dried sample at 1000 °C for 2 h. Major element data were recalculated to an anhydrous (LOI-free) basis and adjusted to 100% before using them in various diagrams. For the determination of CaO in the silicate fraction, samples were separately treated with cold 1 M HCl before digestion and were analyzed separately.

4. Results

4.1. Petrography
Petrographic investigation, according to Dott–McBride scheme classification for the Tanis sandstone, shows that the sandstones are mainly quartz arenites (Figure 4a). The sandstones are composed of three components: framework grains, cementing materials, and pores. The framework grains are mainly quartz (94.47% of the rock volume) and less frequently feldspar, rock fragments, and heavy minerals (less than 3.5%). The quartz grains are fine,

Table 1. Distribution of heavy minerals in Pharaonic sandstone monuments of Tall San Al Hagr.

Location	S. no.	Minerals %		Nonopaque minerals % Unstable %						Stable %							O/NO	ZTR	ZTR/PH	EG/PHZTR	RuZI	KSI
		O	NO	AP	Am	Px	Ep	Gt	Sph	Ky	Mo	Si	Ru	St	Tm	Zr						
	S1	61.4	38.6	0.00	0.9	0.00	0.10	0.00	0.00	13.4	0.00	0.00	18.7	4.3	4.2	58.4	1.59	81.30	90.33	0.00	24.3	17.9
	S2	66.4	33.6	1.40	1.7	0.80	0.90	3.90	0.00	9.2	0.00	0.00	17.2	8.2	2.6	54.1	1.98	73.90	29.56	0.06	24.1	19.1
	S3	65.7	34.3	0.00	1.1	0.20	0.70	0.00	0.00	6.50	0.00	0.00	18.60	4.40	7.10	61.40	1.92	87.10	67.00	0.01	23.3	11.1
	S4	67.7	32.3	0.40	0.5	0.00	3.30	1.30	0.00	8.80	0.00	0.00	17.90	4.20	5.70	57.90	2.10	81.50	163.00	0.06	23.6	13.8
	S5	70.8	29.2	0.60	1.9	1.00	0.90	0.90	0.00	12.9	2.50	0.00	10.80	4.20	4.40	59.90	2.42	75.10	25.90	0.02	15.3	18.5
	S6	69.4	30.6	0.30	0.2	0.00	0.00	1.10	0.00	16.5	0.20	0.00	16.90	5.20	3.80	55.80	2.27	76.50	382.50	0.01	23.2	22.1
	S7	62.6	37.4	0.80	0.4	0.00	1.20	0.40	0.00	12.4	1.60	0.00	19.10	4.60	4.80	54.70	1.67	78.60	196.50	0.02	25.9	17.8
	S8	61.4	38.6	0.00	0.4	0.10	1.20	0.60	0.00	8.10	0.00	0.00	21.60	3.70	3.80	60.50	1.59	85.90	171.80	0.02	26.3	12.1
	S9	60.2	39.8	0.70	0.3	0.00	0.30	0.10	0.00	11.5	0.00	0.00	18.40	7.20	3.80	57.70	1.51	79.90	266.33	0.00	24.2	19.0
	S10	69.4	30.6	0.80	0.9	0.10	2.30	0.80	0.00	11.6	0.00	0.00	16.70	4.00	4.10	58.70	2.27	79.50	79.50	0.04	22.1	16.4
	S11	67.7	32.3	0.30	0.1	0.00	0.00	0.00	0.00	11.5	0.00	0.00	18.90	5.90	5.70	57.60	2.10	82.20	822.00	0.00	24.7	17.5
	S12	67.1	32.9	0.00	0.4	0.00	0.00	1.20	0.00	13.8	0.00	0.00	17.90	4.80	2.80	59.10	2.04	79.80	199.50	0.01	23.2	18.9
	S13	63.7	36.3	0.50	0.70	0.03	0.90	0.30	0.00	12.2	0.00	0.00	17.93	5.17	4.03	58.27	1.75	80.23	109.41	0.01	0.73	1.90
	S14	67.9	32.1	0.83	0.90	0.30	1.07	1.57	0.00	10.8	0.00	0.00	17.60	6.03	4.13	56.80	2.11	78.53	65.44	0.03	1.20	3.53
	S15	66.9	33.1	0.10	0.53	0.07	0.23	0.40	0.00	10.6	0.00	0.00	18.47	5.03	5.20	59.37	2.02	83.03	138.39	0.01	0.60	1.17
	S16	66.2	33.8	0.30	0.53	0.01	1.40	0.93	0.00	11.6	0.00	0.00	17.91	4.72	4.18	58.42	1.95	80.51	147.88	0.03	0.54	2.87
	S17	67.5	32.5	0.64	1.17	0.44	0.96	0.92	0.00	11.9	0.83	0.00	15.44	5.13	4.19	58.32	2.07	77.96	48.39	0.02	1.61	3.04
	S18	68.1	31.9	0.41	0.54	0.12	0.43	1.02	0.00	12.6	0.07	0.00	17.66	5.42	4.38	57.32	2.13	79.36	119.03	0.02	0.67	2.00
	S19	65.2	34.8	0.40	0.49	0.03	0.94	0.58	0.00	11.5	0.53	0.00	18.49	4.79	4.73	57.50	1.87	80.71	156.78	0.02	0.51	2.01
	S20	65.0	35.0	0.31	0.70	0.19	1.19	0.82	0.00	10.5	0.28	0.00	18.32	4.52	4.06	59.08	1.86	81.46	92.02	0.02	0.89	2.70
	Min.	60.2	29.2	0.00	0.1	0.00	0.00	0.00	0.00	6.50	0.00	0.00	10.80	3.70	2.60	54.10	1.51	73.90	25.90	0.00	15.28	11.12
	Max	70.8	39.8	1.40	1.9	1.00	3.30	3.90	0.00	16.5	2.50	0.00	21.60	8.20	7.10	61.40	2.42	87.10	822.00	0.06	26.31	22.10
	Avg.	65.8	34.2	0.44	0.7	0.18	0.91	0.86	0.00	11.4	0.36	0.00	17.73	5.06	4.40	57.98	1.95	80.11	207.83	0.02	23.35	17.01

Location: Tall San Al Hagr
Descriptive statistics: Tall San Al Hagr

O = Opaques; NO = nonopaques; Ap = apatite; Am = amphibole (hornblende); Px = clinopyroxene; Ep = epidote; Gt = garnet; Sph = sphene; Ky = kyanite; Mo = monazite; Si = sillimanite; Ru = rutile; St = staurolite; Tm = tourmaline; Zr = zircon; ZTR = zircon + tourmaline + rutile; PH = pyroxene + hornblende; EG = epidote + garnet; RuZI = (rutile:zircon index) = $100 \times Ru/(Ru + Zr)$; KSi (kyanite-sillimanite-staurolite index) = $100 \times (Ky + Si + St)/(Ky + St + Ru + Tm + Zr)$.

Table 2. Textural data, detrital modes, and QFL indices of the Tall San Al Hagr Pharaonic sandstones.

S. no.	Avg. grain size	Grain roundness	Grain sorting	Grain contact	Quartz Qm	Quartz Qp	Feldspar KF	Feldspar PF	RF Lp	RF Lv	RF Ls	H.m	Gl	Bio	clays	QFL% Qt	QFL% F	QFL% L	QmFLt% Qm	QmFLt% F	QmFLt% Lt	Cement and/or matrix
S1	M	SR-R	WS	C > P	96	0.7	0	0	0	0	0.3	2.9	0	0	0.1	99.69	0.00	0.31	96.00	0.00	1.01	2.73
S2	M-C	SR-R	WS	C > P > S	95.3	0.9	Tr	0	0	0	0.4	3.4	0	0	Tr	99.59	0.00	0.41	95.30	0.00	1.31	3.28
S3	M-C	SR-R	WS	C > P	94.7	0.9	Tr	0	0	0	0.3	4.1	0	0	Tr	99.69	0.00	0.31	94.70	0.00	1.21	3.77
S4	M-C	SR-R	WS	C > P > S	97.1	0.3	0.1	0	0	0	0.4	2	0	0	0.1	99.49	0.10	0.41	97.10	0.10	0.71	1.7
S5	F-M	SR-R	WS	C > P	98.4	0.2	Tr	0	0	0	0.3	1.1	0	0	0	99.70	0.00	0.30	98.40	0.00	0.50	0.97
S6	VF-M	SA-SR	M-Ws	F > P	66.6	0.2	0	0	0	0	0.1	3.8	3	26.1	0.2	99.85	0.00	0.15	66.60	0.00	0.35	2.86
S7	VF-M	SA-SR	M-Ws	F > P	67.2	0.3	Tr	0	0	0	0.1	4.8	2.4	24.9	0.3	99.85	0.00	0.15	67.20	0.00	0.45	3.66
S8	VF-M	SA-SR	M-Ws	F > P	66.6	0.2	Tr	0	0	0	0.1	4.6	2.6	25.7	0.2	99.85	0.00	0.15	66.60	0.00	0.35	3.42
S9	F-M	SR-R	MS	C > P	85.9	8.5	0.1	0	0	0	0.1	5.3	0	0	0.1	99.79	0.11	0.11	85.90	0.11	8.61	12.21
S10	M-VC	SR-R	MS	C > P	90.2	8.7	Tr	0	0	0	0.1	1	0	0	Tr	99.90	0.00	0.10	90.20	0.00	8.80	9.4
S11	M-VC	SR-R	WS	C > P	91	7.8	0.1	0	0	0	0.1	1	0	0	Tr	99.80	0.10	0.10	91.00	0.10	7.90	8.5
S12	M-VC	SR-R	WS	C > P	90.3	8.3	Tr	0	0	0	0.2	1.2	0	0	0	99.80	0.00	0.20	90.30	0.00	8.50	9.14
S13	F-M	SR-R	WS	C > P	93.8	0.6	Tr	0	0	0	0.3	4.1	1.2	0	Tr	99.68	0.00	0.32	99.05	0.00	0.95	3.47
S14	VF-M	SA-SR	M-Ps	F > P	92.4	0.6	Tr	0	0	0	0.2	4.3	1.3	1.2	Tr	99.79	0.00	0.21	99.14	0.00	0.86	3.61
S15	F-M	SR-R	WS	C > P	91.3	4.4	0.1	0	0	0	0.3	3.7	0	0.1	0.1	99.58	0.11	0.31	95.01	0.11	4.88	6.99
S16	M-VC	SR-R	WS	C > P	94.2	4.4	Tr	0	0	0	0.2	1.1	0	0.1	Tr	99.80	0.00	0.20	95.34	0.00	4.66	5.17
S17	M-VC	SR-R	WS	C > P	91.9	4	0.1	0	0	0	0.1	0.6	1.5	0	Tr	99.79	0.11	0.10	95.62	0.11	4.27	4.42
S18	M-VC	SR-R	WS	C > P	91.1	4.3	Tr	0	0	0	0.2	3	1.2	0	0.2	99.79	0.00	0.21	95.29	0.00	4.71	6.4
S19	VF-M	SA-SR	M-Ps	F > P	91.8	0.4	Tr	0	0	0	0.2	4.3	1.9	1.4	Tr	99.78	0.00	0.22	99.35	0.00	0.65	3.41
S20	F-M	SR-R	WS	C > P	89.1	4.5	Tr	0	0	0	0.2	4.7	0.6	0.9	Tr	99.79	0.00	0.21	94.98	0.00	5.02	7.79
Range					66.6-98.4	0.2-8.7	0-0.1	0	0	0	0.1-0.4	0.6-5.3	0-3.0	0-26.1	0-0.3	99.4-99.9	0-0.11	0-8.0	66.6-98.4	0-0.11	0.3-8.8	2.4-38.2
Average					86.61	3.08	0.06	0.00	0.00	0.00	0.21	3.05	0.67	6.39	0.13	99.75	0.03	0.23	86.61	0.03	3.31	11.41

Tall San Al Hagr

VF-M = Fine to medium; F-M = fine to medium; M-VC = medium to very coarse; SR-R = subrounded to rounded; SA-SR = subangular to subrounded; Ws = well sorted; M-Ws = moderate to well sorted; Ms = moderately sorted; C > P = concave-convex contact; C > P > S = concave-convex contact > point contact; F > P = float contact > point contact; Qm = monocrystalline quartz; Qp = polycrystalline quartz; KF = K-feldspar; PF = plagioclase; Lp = plutonic lithic fragment; Lv = volcanic lithic fragment; Ls = sedimentary lithic fragment; H.m = heavy minerals; Gl = glauconite; Bio = bioclasts; Qt = total quartz; F = feldspar; Lt = total Lithic fragment; Qt = Qm + Qp; F = PF + KF; L = Lp + Lv + Ls; Lt = L + Qp.
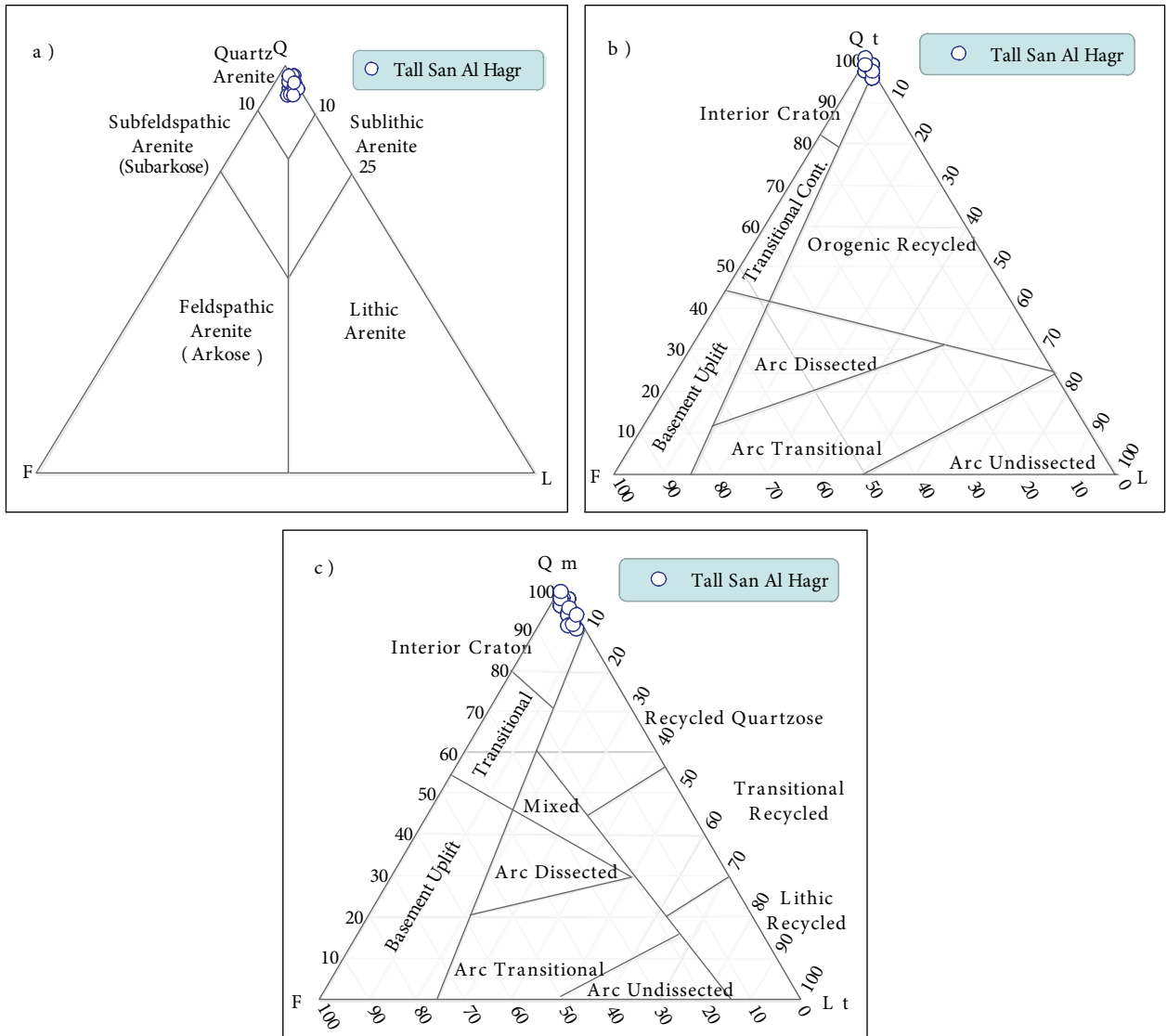
Figure. 4. (a) QFL triangular diagram shows the classification of the Tanis sandstones, modified from Dott (1964) and McBride (1963). **(b)** QtFL and **(c)** QmFLt ternary diagrams for the Tanis sandstones, after Dickinson et al. (1983).

medium to coarse, rounded to subrounded, and moderately well sorted (Figure 5a). It shows point, long to concave-convex, and suture grain contacts (Figure 5b; Table 2). However, an abundance of long contact was noted. Some of the quartz grains show multiple deformation fractures (fr) (Figure 5c). Among quartz grains, Qm (avg. 96.85%) is dominant over Qp (avg. 3.15%). Monocrystalline quartz (Qm) grains exhibit unit extinction and a few of them display undulose extinction (Figure 5d). Qp grains are composed mainly of nonoriented crystallites, commonly with two, three, five, or more crystals per grain with straight to crenulated intercrystal boundaries (Figure 5e). In most samples, microcrystalline quartz (MQ) fringe cement filled up the interstitial space between quartz grains

(Figure 5f). Inclusions are present within both Qm and Qp grains, but they are more common in Qm. They include zircon, tourmaline, and rutile. The XRD study (Figure 6) revealed that the Tanis sandstones are composed mainly of quartz with small percentages of silica, iron oxide, calcite, and dolomite cements, which supports the petrographic examinations.

Feldspars and rock fragments make up less than 0.3% of all samples and are mostly absent in many thin sections. When present they are cloudy and show evidence of dissolution. Feldspar grains are present only as K-feldspar, which is mostly orthoclase and microperthite, while rock fragments include chert, carbonate (shell), and metamorphic (Qp) fragments (Figures 5d and 5e).
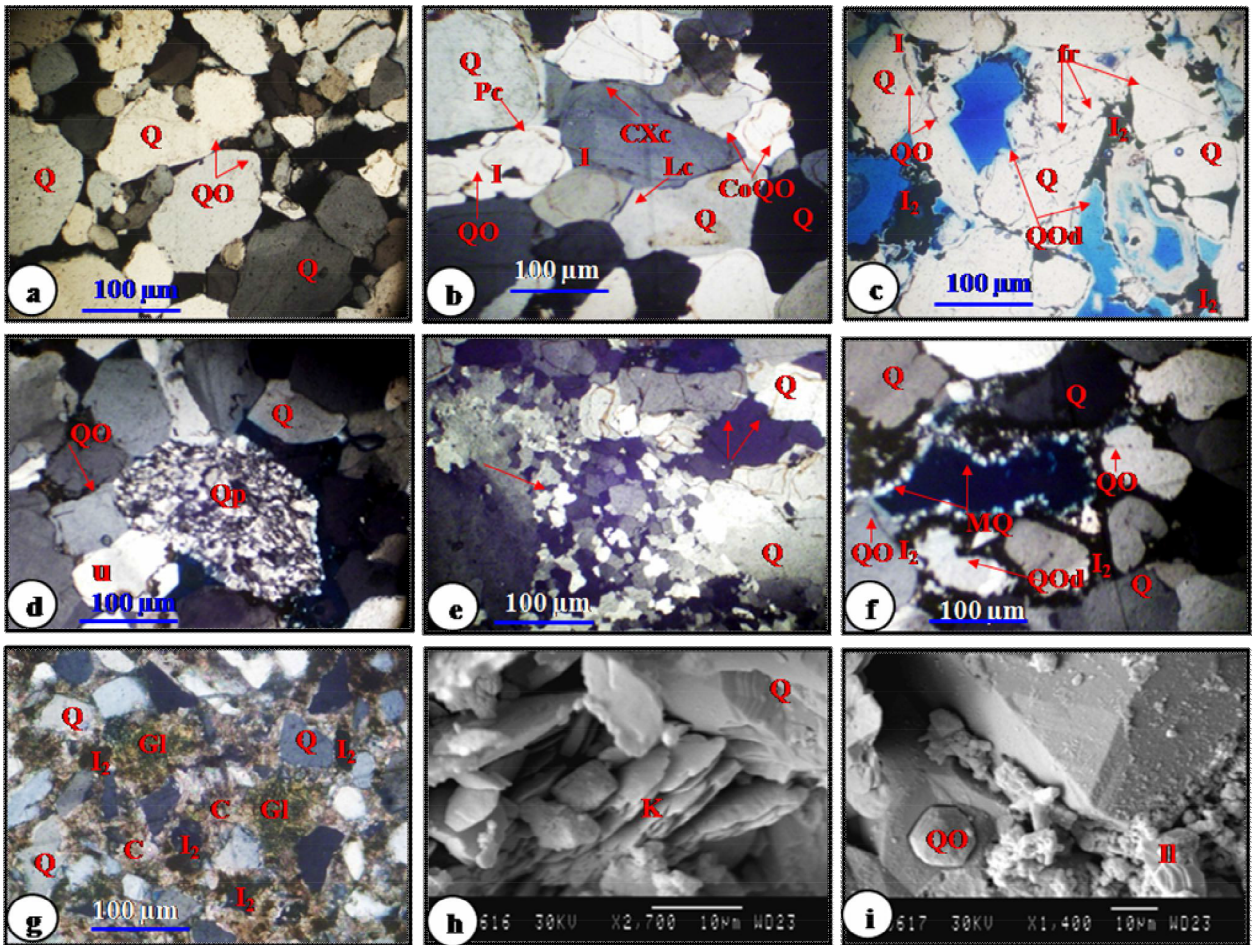
Figure 5. Photomicrograph and SEM of Tanis quartz arenites showing: **(a)** quartz grains (Q) that are medium- to coarse-grained, rounded to subrounded, moderately well sorted, and well cemented with quartz (QO); **(b)** point (Pc), long (Lc), and concave convex contact (CXc) (note: Quartz overgrowth (QO) engulfs and thus postdates iron oxide (I) and coaxial crystal overgrowth (CoQO)); **(c)** silica overgrowths (QO) that were corroded and/or dissolved (QOd) and partially stained and replaced by the second generation of iron oxide (I_2) cement (note: silica dissolution after iron oxide and quartz overgrowth and deformation fractures (fr)); **(d)** polycrystalline quartz grain (Qp) displaying a bimodal size distribution of subcrystals (note: undulose extinction (u) and incipient overgrowth); **(e)** polycrystalline quartz grain consisting of elongate subcrystals with suture and crenulated intercrystalline boundaries (see arrows); **(f)** microcrystalline quartz (MQ) fringe cement that filled up the interstitial space between quartz grains (note: quartz overgrowth dissolution (QOd) and stained iron oxide (I_2) cement); **(g)** detrital quartz (Q) and glauconite pellets (Gl) well cemented by Fe-calcite cement (C) and stained by iron oxide cement (I_2); **(h)** pore-filler kaolinite that occurs between quartz grains; **(i)** silica overgrowths and pore-filling illite (Il).

Volcanic (Lv) and plutonic (Lp) fragments are completely absent in Tanis sandstones. Generally, the fragments are subrounded; however, a few rounded clasts are observed. The absence of feldspars in most samples indicates that the rock is chemically weathered and recycled.

Glauconite is a minor accessory grain type within the samples. Grains are fine-medium to coarse-grained, green to greenish brown, and replaced by pyrite in some samples (Figure 5g).

Heavy minerals form a minor constituent (0.6%–5.3%) of the sandstones and include rounded to well-rounded grains of zircon, rutile, kyanite, staurolite, tourmaline, epidote, garnet, hornblende, and opaque minerals (Table 1). The dominant accessory heavy minerals are composed mainly of opaque minerals. Grains of heavy minerals are very fine and show moderate abrasion. The assemblage is suggestive of mixed sedimentary (reworked), igneous, and metamorphic sources. Cementing materials occurring as pore fillings are silica, calcite, and iron oxides, with siliceous cement being predominant. A portion of oversized pores (2%) is presumed to be due to the dissolution of feldspars, authigenic silica, and other unstable minerals.
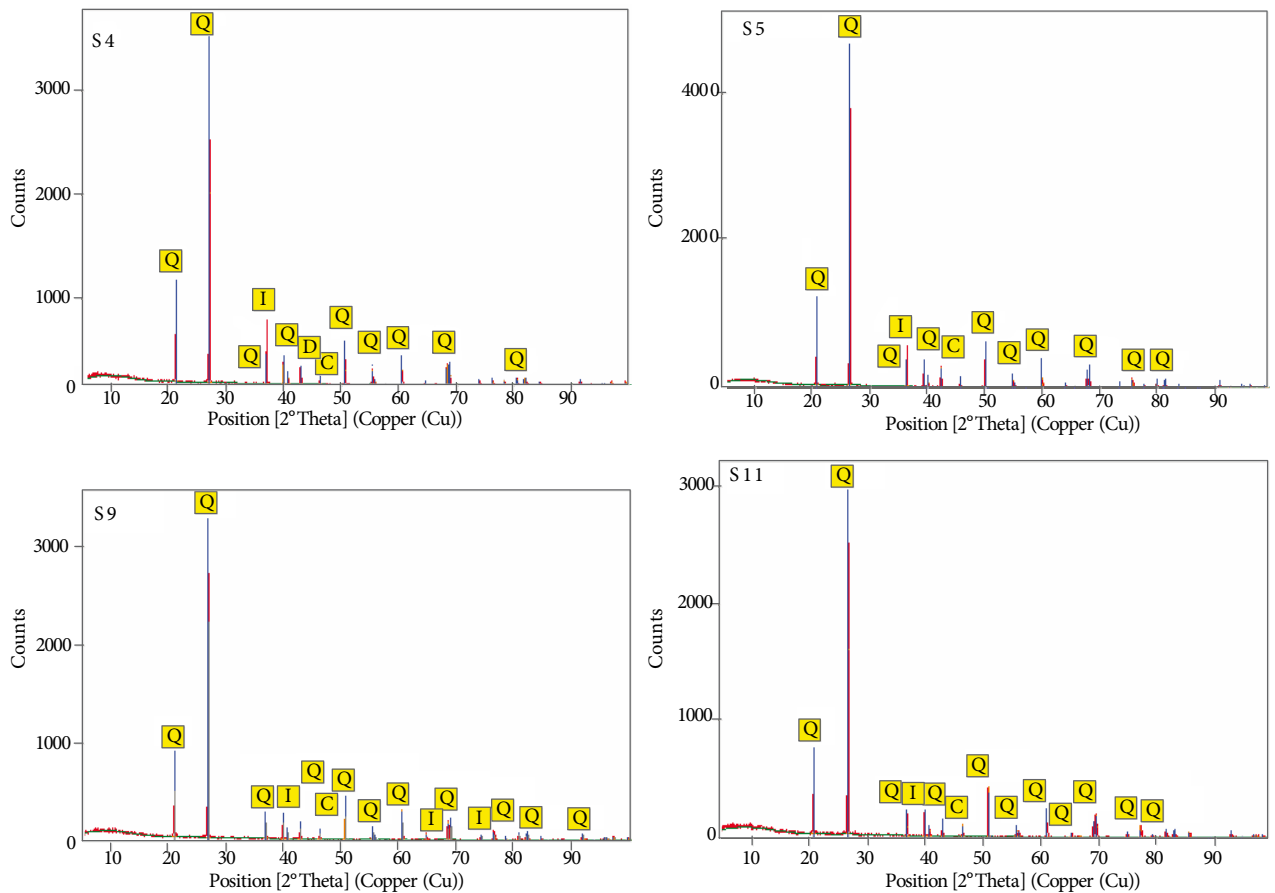
Figure 6. X-ray diffraction patterns of the Tanis sandstone samples. Q = Quartz; I = iron oxide; D = dolomite; C = calcite.

Petrographic and SEM analysis suggests that the vast majority of interstitial clays are of detrital origin. The moderate crystallinity exhibited by the clay minerals indicates their detrital origin from weathering horizons and soils developed on silicic rocks, and transportation in a fluvial environment (Keller, 1956; Abu-Zeid et al., 1989, 1991). The predominance of kaolinite with little illite (Figures 5h and 5i) indicates their sedimentary origin under continental conditions (Lonnie, 1982; Tsuzuki and Kawabe, 1983; Amer et al., 1989).

4.2. Major element geochemistry

The major element concentrations of the Tanis sandstones are given in Table 3. The Tanis sandstone is highly depleted of most of the major elements except SiO_2 (due to enrichment in quartz) and $Fe_2O_3^t$ (due to abundances of iron oxide heavy minerals), suggesting an intense degree of weathering and reworking that removed ferromagnesian minerals and feldspars. Using the geochemical classification diagram of Herron (1988), the Tanis sandstones are classified as quartz arenite (Figure 7), which is also consistent with the petrographic data. The

depletion of Na_2O content for the Tanis sandstones (0.06 ± 0.02, n = 20) can be attributed to a relative absence of plagioclase in them, consistent with the petrographic data. K_2O and Na_2O contents and their ratios also are consistent with the petrographic observations.

The correlation between SiO_2 and Al_2O_3 is negative for the studied sandstones (r = –0.993, n = 20), indicating that much of the SiO_2 is present as quartz grains (Ahmad and Chandra, 2013).

The similarity among other major elements like P_2O_5, MgO, Fe_2O_3, K_2O, Na_2O, and TiO_2 of Tanis sandstone samples (Table 3) indicates a single source rock. The correlation between Fe_2O_3 and TiO_2 is positive (r = 0.69, n = 20), which reveals the presence of Fe and Ti-bearing minerals.

4.3. Trace element geochemistry

Trace element concentrations of the Tanis sandstones are reported in Table 4. The Tanis sandstones are higher in Zr and Ba, compared to other trace elements. The variations in trace element contents among the studied samples are probably due to the sorting effect of sandstones.

Table 3. Major element concentrations (wt.%) of Pharaonic sandstone monuments in Tall San Al Hagr.

Location	Tell San Al Hagr																				Statistical parameters		
	S1	S2	S3	S4	S5	S6	S7	S8	S9	S10	S11	S12	S13	S14	S15	S16	S17	S18	S19	S20	n	mean	std
$(SiO_2)_{adj}$	97.24	96.38	96.66	97.04	96.75	97.25	97.24	97.22	95.45	96.93	97.10	97.75	96.95	96.84	96.73	96.92	96.98	97.24	97.08	96.62	20	96.92	0.46
SiO_2	96.89	96.03	96.16	95.81	96.40	96.60	96.63	96.75	94.33	95.44	96.11	97.24	96.25	96.26	95.89	95.97	96.34	96.59	96.40	95.92	20	96.20	0.61
TiO_2	0.07	0.09	0.10	0.11	0.12	0.08	0.07	0.11	0.10	0.11	0.09	0.06	0.09	0.10	0.09	0.11	0.10	0.08	0.09	0.10	20	0.09	0.02
Al_2O_3	1.09	1.53	1.30	1.12	1.16	1.11	1.15	1.12	1.17	1.11	1.10	1.09	1.22	1.26	1.17	1.15	1.16	1.13	1.16	1.18	20	1.17	0.10
$Fe_2O_3^{*}$	1.26	1.13	1.14	1.12	1.19	1.06	0.96	1.16	2.46	1.22	1.13	0.71	1.14	1.14	1.36	1.17	1.13	1.02	1.11	1.47	20	1.20	0.33
MnO	0.01	0.01	0.02	0.02	0.01	0.01	0.02	0.02	0.02	0.01	0.01	0.01	0.01	0.02	0.02	0.01	0.01	0.01	0.02	0.02	20	0.01	0.00
MgO	0.06	0.22	0.24	0.27	0.13	0.14	0.11	0.07	0.14	0.12	0.13	0.06	0.13	0.17	0.18	0.16	0.14	0.12	0.12	0.13	20	0.14	0.05
CaO	0.05	0.06	0.06	0.09	0.06	0.04	0.15	0.06	0.13	0.12	0.16	0.05	0.10	0.09	0.08	0.09	0.09	0.08	0.10	0.09	20	0.09	0.03
Na_2O	0.03	0.11	0.09	0.04	0.12	0.05	0.04	0.04	0.09	0.05	0.04	0.04	0.06	0.07	0.07	0.07	0.07	0.05	0.05	0.07	20	0.06	0.02
K_2O	0.16	0.42	0.34	0.13	0.41	0.21	0.17	0.14	0.35	0.21	0.17	0.16	0.24	0.27	0.25	0.25	0.26	0.20	0.20	0.26	20	0.24	0.08
P_2O_5	0.02	0.04	0.03	0.02	0.04	0.03	0.07	0.05	0.04	0.07	0.04	0.06	0.05	0.04	0.04	0.05	0.04	0.05	0.05	0.04	20	0.04	0.01
LOI	0.36	0.32	0.37	0.63	0.36	0.37	0.33	0.38	1.16	1.06	0.56	0.36	0.52	0.41	0.63	0.64	0.42	0.42	0.47	0.59	20	0.52	0.23
Total	100.00	99.96	99.85	99.36	100.00	99.70	99.70	99.90	99.99	99.52	99.54	99.84	99.80	99.81	99.76	99.67	99.76	99.75	99.77	99.87	20	99.78	0.17
CaO^{*}	0.05	0.06	0.06	0.09	0.06	0.04	0.15	0.06	0.13	0.12	0.16	0.05	0.10	0.09	0.08	0.09	0.09	0.08	0.10	0.09	20	0.09	0.03
CIA	77.42	66.93	67.21	74.97	60.38	74.10	68.55	77.22	60.22	67.53	66.84	76.53	69.57	69.02	68.87	67.67	67.20	71.76	70.50	67.82	20	69.52	4.78
CIW	88.59	84.05	83.48	82.98	79.09	87.74	77.23	86.48	75.25	78.68	75.49	87.42	82.01	82.38	81.98	80.67	80.97	83.27	81.44	81.04	20	82.01	3.76
ICV	1.50	1.33	1.53	1.59	1.76	1.43	1.32	1.43	2.81	1.66	1.57	1.00	1.44	1.46	1.74	1.61	1.55	1.38	1.45	1.81	20	1.57	0.34
Al_2O_3/TiO_2	15.57	17.00	13.00	10.18	9.67	13.88	16.43	10.18	11.70	10.09	12.22	18.17	14.35	12.95	12.65	10.85	11.95	14.94	12.51	11.65	20	13.00	2.44
K_2O/Na_2O	5.33	3.82	3.78	3.25	3.42	4.20	4.25	3.50	3.89	4.20	4.25	4.00	4.17	3.82	3.77	3.70	3.78	4.03	3.90	3.78	20	3.94	0.43
SiO_2/Al_2O_3	88.89	62.76	73.97	85.54	83.10	87.03	84.03	86.38	80.62	85.98	87.37	89.21	78.89	76.25	81.95	83.27	83.19	85.48	83.06	81.45	20	82.42	6.06

$(SiO_2)adj$ = Major element data were recalculated to anhydrous (LOI-free) basis and adjusted to 100%; $Fe_2O_3^{*}$ = total Fe expressed as Fe_2O_3; n = number of samples; std = standard deviation; CIA = $[Al_2O_3/(Al_2O_3 + CaO^{*} + Na_2O + K_2O)] \times 100$; CIW = $[Al_2O_3/(Al_2O_3 + CaO^{*} + Na_2O)] \times 100$ (Nesbitt and Young, 1982). CaO^{*} = CaO in silicate phase. To calculate CaO^{*}, the assumption proposed by McLennan et al. (1993) was followed. ICV = $(Fe_2O_3 + K_2O + Na_2O + CaO + MgO + MnO + TiO_2)/Al_2O_3$ (Cox et al., 1995).
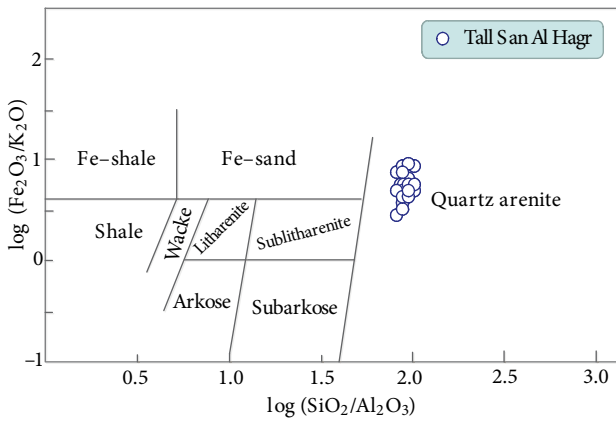
Figure 7. Chemical classification of the Tanis sandstones based on log (SiO_2/Al_2O_3) vs. log (Fe_2O_3/K_2O) diagram of Herron (1988).

In comparison with average upper continental crust (UCC), the Tanis sandstones are depleted in V, Pb, Sc, U, Th, and Rb and enriched in most trace elements (Figure 8). The average relative concentration ratios lie between 1 and 10. The Tanis sandstones are enriched in high-strength elements like Zr and Hf, which is probably due to the abundance of heavy mineral zircon.

Most trace elements except Ni, Co, Cr, Pb, and Ga show statistically significant correlation with TiO_2, Al_2O_3, Fe_2O_3, Na_2O, and K_2O, indicating that these elements are absorbed into phyllosilicates and/or associated with iron oxide minerals. The Tanis sandstones have low concentrations of transition metals Cr, Co, Ni, and V. These transitional elements are mainly concentrated in the clays or metal oxides (Turekian and Michael, 1960). Vanadium is positively correlated with Fe_2O_3 (r = 0.852, n = 20). It is generally absorbed on kaolinite and possibly associated with iron oxides (Hirst, 1962).

The large ion lithophile elements such as Rb, Cs, Ba, Sr, Th, and U are depleted in the Tanis sandstones and are comparable to UCC (Figure 8), which may reflect a high degree of weathering and recycling.

5. Discussion

5.1. Tectonic setting

Dickinson and Suczek (1979) and Dickinson et al. (1983) related detrital sandstone compositions to major provenance types such as stable cratons, basement uplifts, magmatic arcs, and recycled orogens. To interpret the tectonic environment, the Tanis sandstones were plotted on the QtFL and QmFLt ternary diagrams of Dickson et al. (1983). The Tanis sandstones are plotted in a cratonic interior field (Figures 4b and 4c), which reflects mature sandstones derived from relatively low-lying granitoid and gneissic sources, supplemented by recycled sands from associated platform or passive margin basins (Dickson et al., 1983). The scarcity of unstable grains (feldspar and other rock fragments) at <0.3% suggests that the source area underwent an intensive chemical weathering in a warm humid climate (Pettijohn et. al., 1987; Amireh, 1991).

The concentration of major elements (Table 3) was used to discriminate the tectonic setting of sandstones (Schwab, 1975; Bhatia, 1983; Roser and Korsch, 1986, 1988; Armstrong-Altrin et al., 2004). The tectonic discrimination diagrams proposed by Bhatia (1983) and Roser and Korsch (1986, 1988) have mostly been used to identify the tectonic setting of unknown basins (Jafarzadeh et al., 2013; Nowrouzi et al., 2013).

The discriminant function diagram of Roser and Korsch (1988) suggests that Tanis sandstones may derive mainly from mature polycyclic continental sedimentary rocks (Figure 9a). The discrimination diagram of Bhatia (1983)
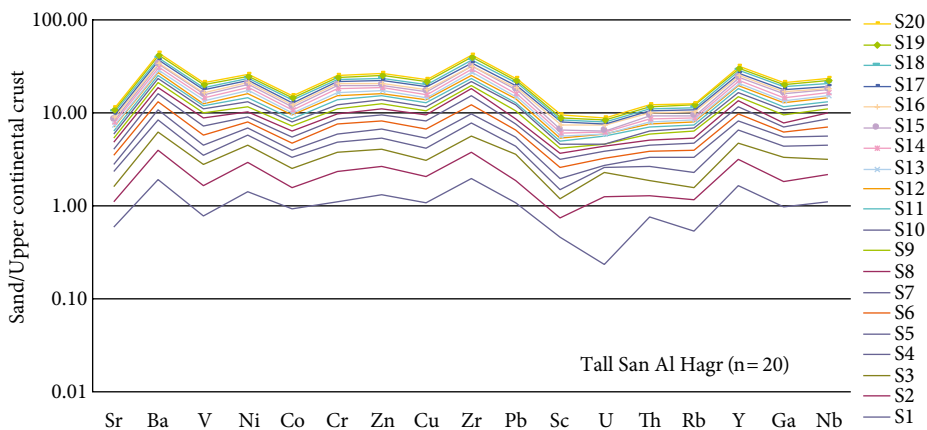

Figure 8. Multielement normalized diagram for the Tanis sandstone samples, normalized against average upper continental crust (Taylor and McLennan, 1985). A horizontal line for sand/upper continental crust value of 1 is included for reference.

Table 4. Trace element concentrations (ppm) of Pharaonic sandstone monuments in Tall San Al Hagr.

| Location	Tell San Al Hagr																				Statistical parameters		
	S1	S2	S3	S4	S5	S6	S7	S8	S9	S10	S11	S12	S13	S14	S15	S16	S17	S18	S19	S20	n	mean	std
Sr	3.8	3.1	3.2	5.0	3.0	4.3	4.1	5.2	3.0	3.3	3.0	4.0	3.6	3.6	3.8	3.7	3.5	4.1	4.1	3.8	20	3.8	0.6
Ba	74.0	98.0	144.0	142.0	217.0	303.0	439.0	371.0	168.0	145.2	96.0	71.0	189.1	177.3	131.3	173.3	198.3	236.1	293.1	228.6	20	194.8	96.7
V	5.8	7.2	13.0	5.0	8.0	21.0	29.0	25.0	16.0	12.7	7.0	5.0	13.7	13.1	9.8	9.8	12.3	16.2	19.4	16.6	20	13.3	6.6
Ni	25.0	29.4	32.0	16.0	16.0	11.0	12.0	11.5	27.0	31.4	30.0	24.0	24.4	25.7	24.8	21.9	20.7	17.9	17.5	21.2	20	22.0	6.5
Co	8.0	4.3	9.0	6.0	4.0	5.0	7.0	6.0	7.0	5.0	5.0	7.0	6.1	6.1	7.3	5.3	5.0	6.6	6.1	6.0	20	6.1	1.2
Cr	12.0	16.0	25.0	11.0	13.0	35.0	11.0	16.0	13.0	16.0	37.0	20.0	42.0	38.4	29.5	20.5	10.9	23.9	22.4	19.6	20	21.6	9.9
Zn	18.7	21.3	23.0	18.0	18.0	35.0	23.0	29.0	21.0	23.1	21.0	18.0	21.5	23.6	20.0	20.2	24.4	24.0	23.4	24.5	20	22.5	4.0
Cu	11.0	9.1	11.0	11.0	12.0	25.0	24.0	25.0	11.0	11.0	9.0	14.0	13.8	13.5	11.8	11.9	14.9	18.7	18.7	16.1	20	14.6	5.1
Zr	81.9	60.3	66.8	112.0	75.0	399.0	672.0	535.0	62.0	67.1	60.0	80.0	220.3	180.5	80.2	118.6	178.6	307.8	386.5	239.0	20	199.1	176.2
Pb	11.0	6.0	44.2	6.0	11.0	11.0	10.0	11.0	73.0	43.5	6.0	11.0	17.6	16.8	33.6	19.5	11.2	16.4	14.5	28.0	20	20.1	16.9
Sc	2.8	1.9	2.7	2.0	3.0	3.8	3.7	3.5	3.0	2.6	1.8	2.8	2.8	2.5	2.6	2.6	2.8	3.2	3.1	2.9	20	2.8	0.5
U	1.7	0.9	1.0	1.9	1.4	3.4	3.5	3.3	1.8	1.1	0.9	1.6	1.8	1.5	1.6	1.5	1.8	2.5	2.5	2.1	20	1.9	0.8
Th	5.5	3.3	3.7	6.2	4.1	3.2	4.2	3.9	5.9	3.7	3.3	4.4	4.2	3.5	5.0	4.5	3.5	4.2	4.2	4.2	20	4.2	0.8
Rb	3.3	4.1	2.4	5.0	1.0	5.0	4.9	4.2	1.0	2.8	4.0	3.0	3.8	3.7	2.9	3.1	3.4	3.9	4.0	3.1	20	3.4	1.1
Y	39.8	31.0	32.0	54.0	37.0	40.0	73.0	61.0	29.0	32.5	30.0	40.0	44.1	38.5	38.8	41.9	36.4	47.9	55.0	41.2	20	42.1	11.2
Ga	8.8	7.0	26.0	11.0	12.0	5.0	6.0	5.5	43.0	27.5	7.0	10.0	12.3	11.4	22.5	15.7	8.8	10.9	9.9	17.2	20	13.9	9.4
Nb	12.0	11.0	10.0	20.0	13.0	21.0	36.0	28.0	10.0	11.0	10.0	14.0	17.5	14.8	13.5	15.4	14.7	21.1	24.2	16.9	20	16.7	6.8
Th/U	3.24	3.69	3.87	3.24	2.95	0.94	1.20	1.18	3.29	3.51	3.67	2.75	2.34	2.35	3.22	2.96	1.97	1.67	1.66	2.01	20	2.6	0.9
Zr/Sc	29.25	31.74	24.74	56.00	25.00	105.00	181.62	152.86	20.67	25.42	33.33	28.57	79.83	72.94	30.55	45.62	64.52	95.26	123.08	81.42	20	65.4	46.4
Rb/Sr	0.87	1.32	0.75	1.00	0.33	1.16	1.20	0.81	0.33	0.83	1.33	0.75	1.05	1.01	0.75	0.84	0.98	0.97	0.96	0.80	20	0.9	0.3
Th/Sc	1.96	1.75	1.36	3.08	1.38	0.84	1.14	1.11	1.97	1.40	1.83	1.57	1.51	1.43	1.92	1.75	1.28	1.30	1.34	1.44	20	1.6	0.5
Th/Co	0.69	0.77	0.41	1.03	1.03	0.64	0.60	0.65	0.85	0.74	0.66	0.63	0.69	0.58	0.70	0.86	0.71	0.64	0.69	0.70	20	0.7	0.1
Th/Cr	0.458	0.207	0.147	0.560	0.317	0.091	0.382	0.244	0.455	0.231	0.089	0.220	0.099	0.092	0.171	0.221	0.325	0.176	0.188	0.216	20	0.245	0.1
Cr/Th	2.2	4.8	6.8	1.8	3.2	10.9	2.6	4.1	2.2	4.3	11.2	4.5	10.1	10.8	5.9	4.5	3.1	5.7	5.3	4.6	20	5.4	3.0
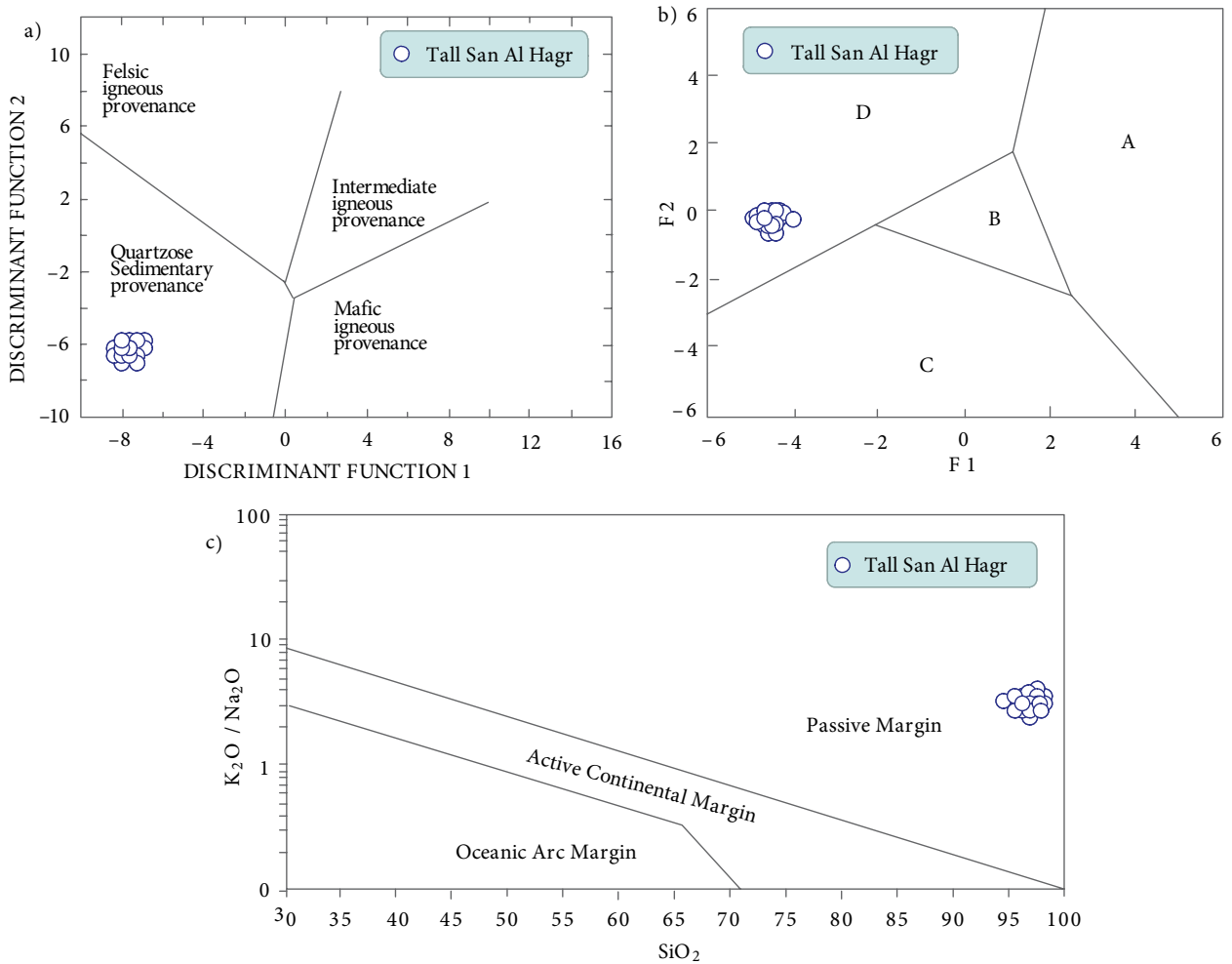
Figure 9. Discrimination function analysis classification plots of the Tanis sandstone: **(a)** Roser and Korsch (1988), **(b)** Bhatia (1983) and **(c)** Roser and Korsch (1986). A: Oceanic island Arc, B: continental island Arc, C: active continental margin, D: passive margin.

favors a passive margin setting for the Tanis sandstone (Figure 9b). The tectonic discrimination diagram of Roser and Korsch, (1986) suggests that the Tanis sandstone falls mainly in the passive margin field (Figure 9c). In a passive margin setting, the sediments are largely quartz-rich, derived from plate interior or stable continental areas and deposited in intracratonic basin (Roser and Korsch, 1986).

However, Armstrong-Altrin and Verma (2005) evaluated these major element-based discrimination diagrams using Miocene to Recent sediments and showed a low percentage success rate (0%–23%) for the Bhatia (1983) diagram and about 31.5%–52.3%) for the Roser and Korsch diagram (1986, 1988). Recently, Verma and Armstrong-Altrin (2013) proposed two new discriminant function-based major element diagrams for the tectonic discrimination of siliciclastic sediments from three main tectonic settings: island or continental arc, continental rift,

and collision, created for the tectonic discrimination of high-silica $[(SiO_2)_{adj} = 63\%–95\%]$ and low-silica rocks $[(SiO_2)_{adj} = 35\%–63\%]$. These two new diagrams were constructed based on worldwide examples of Neogene-Quaternary siliciclastic sediments from known tectonic settings, $\log_e$-ratio transformation of ten major elements with SiO_2 as the common denominator, and linear discriminant analysis of the $\log_e$-transformed ratio data. Armstrong-Altrin (2014) tested these two tectonic discrimination diagrams using geochemistry data of the Holocene (<0.0117–0 Ma) and Precambrian clastic sedimentary rocks (~512–2800 Ma) from various parts of the world. He concluded that the two multidimensional diagrams can be considered as a tool for successfully discriminating the tectonic setting of older sedimentary basins. In addition, these discrimination diagrams were used in recent studies to discriminate the tectonic setting of a source region based on sediment

geochemistry (Armstrong-Altrin et al., 2014; Zaid and Gahtani, 2015). The tectonic discriminant function-based multidimensional diagram for high-silica sediments is used to identify the tectonic environment of the source area.

The new discriminant function-based major element diagram (Figure 10) is used in this study to identify the tectonic environment of the studied Pharaonic sandstones samples of the Tanis archeological site. On the high-silica $[(SiO_2)_{adj} \geq 63\%$ to $95\%]$ tectonic discriminant diagram of Verma and Armstrong-Altrin (2013), the Tanis sandstone falls exclusively in the rift field (Figure 10). The results obtained from this discriminant function-based multidimensional diagram provide good evidence for the source area tectonic system, a rifted margin, which is consistent with the general geology of the Gebel El Ahmar Quarry region (Said, 1990; Knox et al., 2009).

5.2. Source area weathering and sediment recycling

The weathering history of ancient sedimentary rocks can be evaluated in part by examining relationships among the alkali and alkaline earth elements (Nesbitt and Young, 1982). A good measure of the degree of chemical weathering can be obtained by the chemical index of
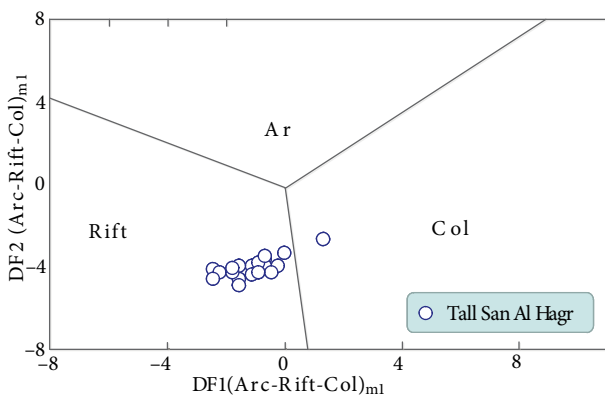
alteration (CIA; Nesbitt and Young, 1982) and chemical index of weathering (CIW; Fedo et al., 1995). High CIA and CIW values (i.e. 75–100) indicate intensive weathering in the source area, whereas low values (i.e. 60) indicate low weathering in the source area. The calculated CIA and CIW values for the Tanis sandstones (Table 3) range from 60.2 to 70.2 (avg. 69.52) and from 75.25 to 87.74 (avg. 82.01; Table 3), respectively. These values (>60) indicate moderate to intensive weathering and reflect warm humid climate conditions in the source area (McLennan et al., 1993).

The CIA values for the Tanis sandstones are plotted in an Al_2O_3-$(CaO^* + Na_2O)$-K_2O (A-CN-K) ternary diagram (molecular proportions, Figure 11). All the samples plot parallel to the Al_2O_3–K_2O edge (Figure 11), supporting the conclusion that the Tanis sandstones were derived from a granite terrain. The samples plot away from the weathering trend, towards the K apex, indicating that the samples are enriched in K_2O and depleted in CaO and Na_2O.

Quartz arenites exhibit comparatively low CIA values (between 60 and 70). In the A-CN-K diagram, most of the sandstone samples fall along the A-K line instead of A-CN. This type of trend is generally found in sedimentary rocks that have undergone K-metasomatism, by which addition of K to weathered residues occurs (Fedo et al., 1995; Nagarajan et al., 2007). Obviously, the highest degree of alteration (in terms of CIA) is compatible with samples high in kaolinite and low in feldspar content.

Petrographic evidence such as heterogeneous roundness for different grains implies the importance of mechanical effects for grain shape configuration. Moreover, the rounded quartz overgrowths indicate recycling, which, in turn, can modify the compositional data towards the

Figure 10. New discriminant-function multidimensional diagram proposed by Verma and Armstrong-Altrin (2013) for high-silica clastic sediments to discriminate three tectonic settings (arc, continental rift, and collision). The subscript $_{m1}$ in DF1 and DF2 represents the high-silica diagram based on $\log_e$-ratios of major elements. The discriminant function equations are:

$DF1_{(Arc-Rift-Col)m1} = (-0.263 \times \ln(TiO_2/SiO_2)_{adj}) + (0.604 \times \ln(Al_2O_3/SiO_2)_{adj}) + (-1.725 \times \ln(Fe_2O_3^t/SiO_2)_{adj}) + (0.660 \times \ln(MnO/SiO_2)_{adj}) + (2.191 \times \ln(MgO/SiO_2)_{adj}) + (0.144 \times \ln(CaO/SiO_2)_{adj}) + (-1.304 \times \ln(Na_2O/SiO_2)_{adj}) + (0.054 \times \ln(K_2O/SiO_2)_{adj}) + (-0.330 \times \ln(P_2O_5/SiO_2)_{adj}) + 1.588.$

$DF2_{(Arc-Rift-Col)m1} = (-1.196 \times \ln(TiO_2/SiO_2)_{adj}) + (1.604 \times \ln(Al_2O_3/SiO_2)_{adj}) + (0.303 \times \ln(Fe_2O_3^t/SiO_2)_{adj}) + (0.436 \times \ln(MnO/SiO_2)_{adj}) + (0.838 \times \ln(MgO/SiO_2)_{adj}) + (-0.407 \times \ln(CaO/SiO_2)_{adj}) + (1.021 \times \ln(Na_2O/SiO_2)_{adj}) + (-1.706 \times \ln(K_2O/SiO_2)_{adj}) + (-0.126 \times \ln(P_2O_5/SiO_2)_{adj}) - 1.068.$
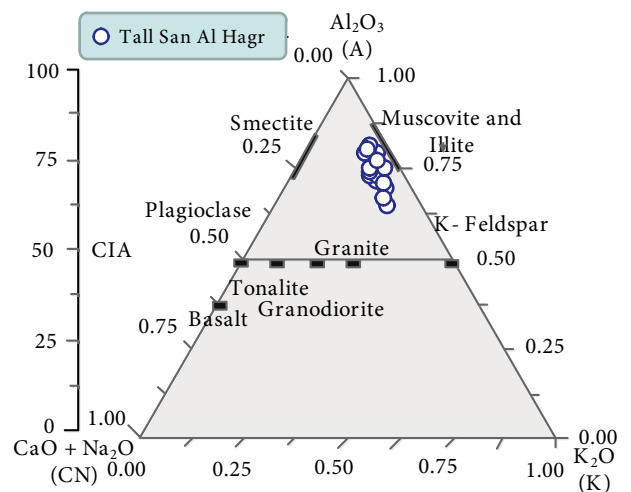

Figure 11. A–CN–K ternary diagram of molecular proportions of Al_2O_3 – $(CaO^* + Na_2O)$ – K_2O, after Nesbitt and Young (1982).

quartz-rich sandstones. The sparse sedimentary rock fragments and coaxial crystal overgrowth (i.e. double, triple overgrowth) on quartz grains (Figure 5c) indicate several phases of recycling from older sedimentary sources (Al-Habri and Khan, 2008).

To identify the maturity of sandstones, the ratio of SiO_2/Al_2O_3 against that of quartz, quartzite, and chert / (feldspar + rock fragments) (Q/F+RF) was plotted (Figure 12a) (Pettijohn, 1975). A higher SiO_2 ratio coincides with higher silica phases of quartz, quartzite, and chert, which in turn reflect high maturity. The bivariate plot of SiO_2 against total $Al_2O_3+K_2O+Na_2O$ proposed by Suttner and Dutta (1986) was used in order to identify the maturity of the Tanis sandstones as a function of climate (Figure 12b). This plot revealed a humid climatic condition in the source area for the samples investigated.

5.3. Provenance

The provenances of clastic rocks have been determined by petrography, including investigation of the undulosity and polycrystallinity of quartz grains (Basu et al., 1975; Yong, 1976), feldspar types (Pittman, 1970), rock fragments (Pettijohn et al., 1987), and heavy mineral types (Morton, 1985; Asiedu et al., 2000).

The dominance of monocrystalline quartz grains indicate that the sediments were derived from a granitic source (Basu et al., 1975). Dabbagh and Rogers (1983) also suggested that such grains may be the result of the disaggregation of original polycrystalline quartz during high-energy or long-distance transport from the metamorphic source. Polycrystalline quartz grains are commonly of two types: the first type is composed of two, three, five, or more crystals per grain with straight to slightly curved intercrystal boundaries (Figure 5d). The second type consists of polycrystalline quartz grains composed of more than five elongate crystals, exhibiting irregular to crenulated intercrystal boundaries (Figure 5e). The first type suggests an origin from plutonic igneous rocks (Folk, 1974; Blatt et al., 1980), while the second type indicates an origin from metamorphic source rocks (Blatt et al., 1980; Asiedu et al., 2000). Some polycrystalline quartz grains show a bimodal size distribution (Figure 5e), which indicates a gneissose source (Blatt et al., 1980). A few quartz grains have incipient silica overgrowths (Figure 5d) as the result of pressure dissolution at the grain contacts indicated by the occurrence of concave-convex and sutured grain to grain contacts (Pettijohn et al., 1987).

Abundance of zircon, rutile, and epidote indicates acid to intermediate igneous (plutonic) rocks (Friedman and Sanders, 1978). However, amphiboles, staurolite, and garnet indicate metamorphic rocks (Pettijohn, 1984). The general abundance of the ultrastable heavy minerals, e.g., zircon, tourmaline, and rutile (ZTR), in Tanis sandstone (avg. 80.15; Table 1) indicates intensive chemical weathering in the source area and the recycling of detrital materials. This in turn indicates a high degree of maturity of sandstones (Carver, 1971; Morton, 1985). Additionally,
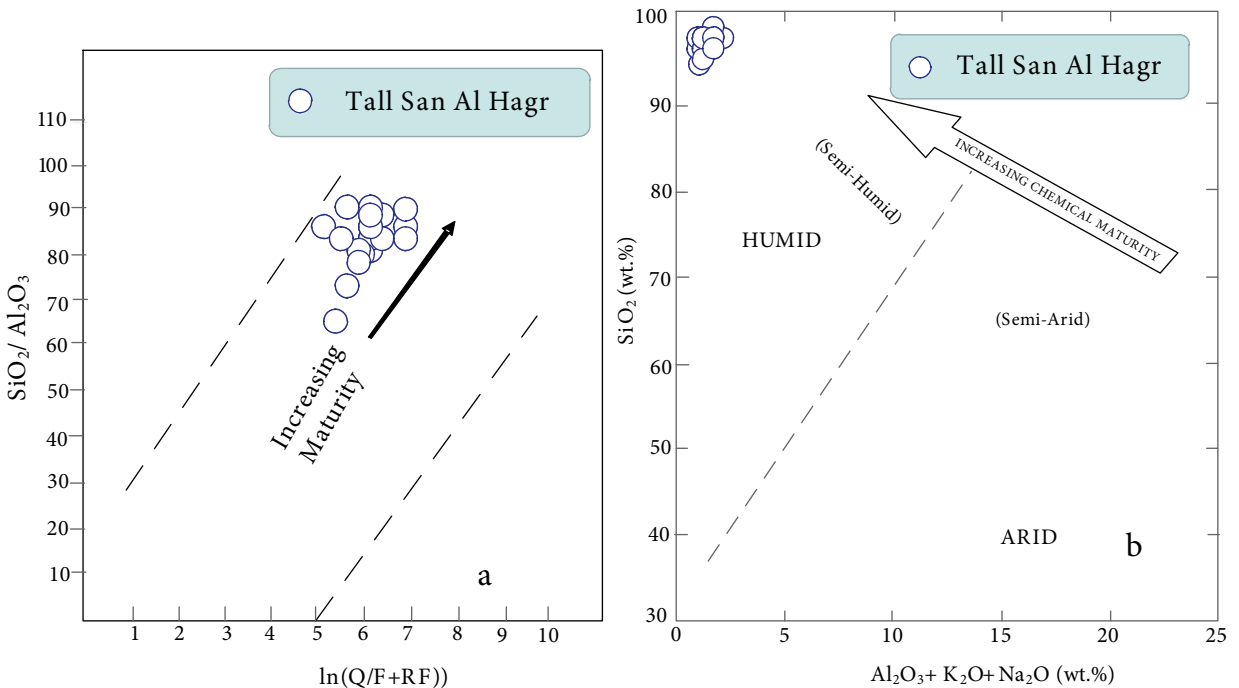

Figure 12. Bivariate plots: **(a)** SiO_2/Al_2O_3 versus $Ln(Q/(F + RF))$, **(b)** SiO_2 versus $Al_2O_3+ K_2O + Na_2O$ (Suttner and Dutta, 1986).

the presence of a high percentage of metastable minerals, e.g., garnet, kyanite, and staurolite, in Tanis sandstone (avg. 17.32; Table 1) signifies a continuous supply of fresh sediments from the Precambrian basement exposure of the Nubian Shield rocks (Dar, 1998).

The major element-based provenance discriminant function diagram of Roser and Korsch (1988) is frequently used by many researchers to identify the provenance of terrigenous sediments (Hofer et al., 2013; Khanchuk et al., 2013; Vdačný et al., 2013; Shadan and Hosseini-Barzi, 2013). This discriminant function diagram reveals that the source sediments of the Tanis sandstone were mature polycyclic continental sedimentary rocks, supporting the interpretation that they were derived from granitic-gneissic source area (Figures 9a and 13a), similar to passive margin sediments (Roser and Korsch, 1986; Kroonenberg, 1994).

The K_2O and Rb contents in terrigenous sediments are sensitive to sedimentary recycling processes and have been widely used as indicators for source composition

(Armstrong-Altrin et al., 2012, 2015; Tao et al., 2013). The K_2O/Al_2O_3 versus Rb/Al_2O_3 bivariate plot reveals the compositional difference among the Tanis sandstone samples (Figure 13b), which varies from intermediate to felsic. Higher values of Cr (>150 ppm) and Ni (>100 ppm) are diagnostic of ultramafic sources (Garver et al., 1996). In the Tanis sandstones, Cr (21.6 ± 9.9) and Ni (22 ± 6.5) are depleted with respect to the average UCC composition (Figure 8). This depletion in Cr, Ni, V, and Co contents (Tables 3 and 5) may suggest a felsic source rock.

Trace element ratios such as Th/Sc, Th/Co, Th/Cr, and Cr/Th are significantly different in mafic and felsic source rocks (Cullers, 2000) and can therefore provide information about the provenance of terrigenous sediments (Armstrong-Altrin et al., 2013). These ratios are compared in Table 5 with those of sediments derived from mafic and felsic source rocks. The trace element ratios of Tanis sandstones fall within the range of sediments derived from felsic source rocks (Table 5).

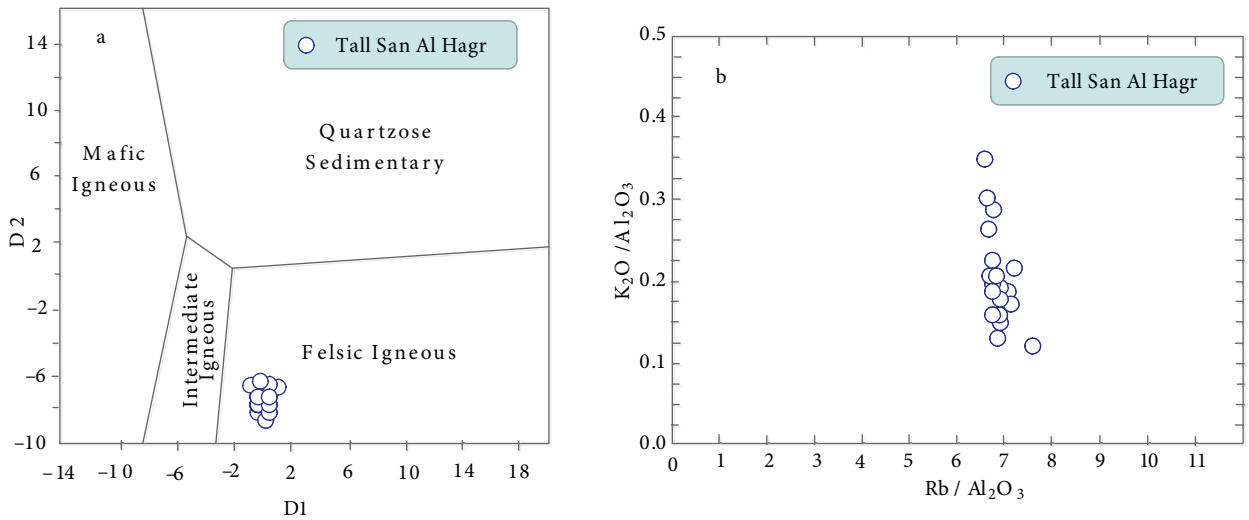The K_2O/Na_2O ratio can be considered as a simplified

Figure 13. (a) Discriminant function diagram using major elements for the Tanis sandstones (Roser and Korsch, 1988); **(b)** K_2O/Al_2O_3 versus Rb/Al_2O_3 bivariate diagram for the Tanis sandstones.

Table 5. Range of elemental ratios of the Pharaonic sandstone monuments in Tall San Al Hagr in this study compared to the ratios in similar fractions derived from felsic, mafic rocks, and upper continental crust.

Elemental ratio	Tanis sandstones		Range of sediment from felsic sources[2]	Range of sediment from mafic sources (Cullers, 1994, 2000; Cullers and Podkovyrov, 2000)	UCC (Taylor and McLennan, 1985)
	Range	Average			
Th/Sc	0.84–3.08	1.6	0.84–20.5	0.05–0.22	0.79
Th/Co	0.41–1.03	0.7	0.67–19.4	0.04–1.40	0.63
Th/Cr	0.09–0.56	0.25	0.13–2.70	0.02–0.05	0.13
Cr/Th	1.79–11.21	5.4	4.0–15.0	25–500	7.76

chemical provenance indicator (Potter, 1978). Higher values of this ratio reflect derivation from felsic rather than from basic rocks. This is also confirmed by the clay mineral content, as illite and kaolinite were considered to be inherited from weathering horizons and soils developed on silicic (granitic) rocks. In addition, the low percentage of smectite and the absence of chlorite also preclude mafic source rocks.

The Proterozoic granites, metagabbros, and metavolcanics could have been the source rocks for Tanis sandstones, which have been uplifted and exposed because of the stress built up by the Rifting Orogeny, initiated during the Oligocene and continuing until the post-Miocene.

5.4. Source quarry
This study also aims to distinguish between the Cairo and Aswan quarries that are the main source quarries of sandstones of archeological sites in Egypt. The true quartzite is restricted to Cairo (Gebel Ahmar) and the Aswan quarries (Harrell and Madbouly, 2006). Heavy mineral fingerprinting can be used to distinguish between the Cairo and Aswan quarries, such as the relative abundance of kyanite and staurolite, both individually and as a group, and can therefore be used to distinguish between the two quarries (Knox et al., 2009). The abundance of kyanite and staurolite in Tanis sandstones (Table 1) is consistent with Cairo (Gebel Ahmar quarry), as might be expected for a site in the Delta area.
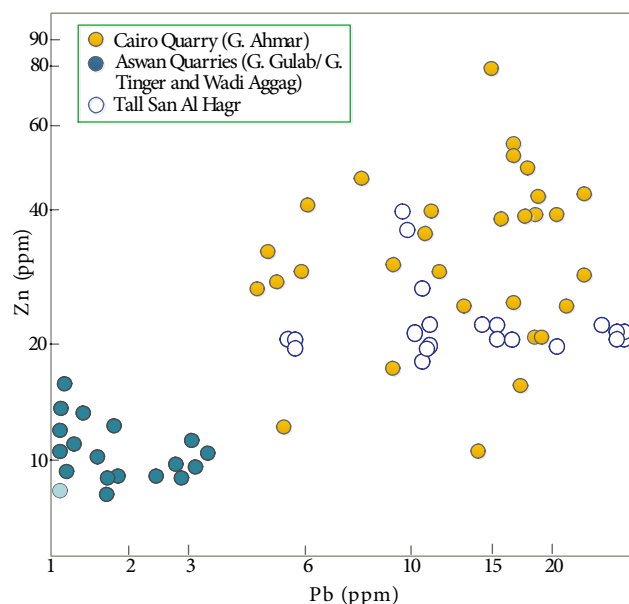

Figure 14. Trace elements for the Tanis sandstones (artifacts of the Ramesses II temple), compared with these for sandstones from Gebel Ahmar and Aswan quarries, after Knox et al. (2009).

In addition, well-developed fringes of microcrystalline quartz cement filled up the interstitial space between quartz grains (Figure 5f), which is generally agreed to be found only at Gebel Ahmar (Knox et al., 2009). Klemm and Klemm (1993, 2001, 2008) stated that the fringe cement is characteristic of the Gebel Ahmar sandstones and that sandstones lacking it must therefore have come from Aswan. The majority of Tanis sandstone samples contain pebbles of chert (finely crystalline quartz), which is consistent only with Gebel Ahmar (Aston et al., 2000). Quartz grains of the Tanis sandstones have a high degree of roundness, which more consistent with the sandstones of Gebel Ahmar than those of the Aswan quarries (Aston et al., 2000).

Because of the difficulty of distinguishing between the two sources quarries for the Tanis sandstones by conventional petrological means, Heizer et al. (1973) proposed that a better approach would be to study their geochemistry. Klemm and Klemm (1993, 2008) showed that the Cairo and Aswan quarries could be distinguished by their differing contents of a wide range of elements (e.g., Co, Fe, Pb, Rb, Sr, and Zr). The Zn versus Pb bivariate plot of Knox et al. (2009) reveals the Gebel Ahmar source quarry for Tanis sandstones (Figure 14).

Finally, this study indicates that the Gebel Ahmar sandstone is the source quarry of Tall San Al Hagr (Tanis) sandstone.

The Tanis sandstones are texturally mature and derived from relatively low-lying deeply weathered granitic-gneissic sources supplemented by recycled sands from an associated platform and were deposited in an intracratonic basin or passive continental margins of a synrift basin. The CIA and CIW values of the Tanis sandstones indicate extensive weathering and may reflect low-relief and warm humid climatic conditions in the source area. The heavy minerals and trace elements revealed that the Cairo (Gebel Ahmar) quarry is the source for Tanis sandstones. The petrographic and geochemical data suggested that the Tanis sandstone and its source quarry of Gebel Ahmar were derived from the Precambrian basement rocks of the northwestern margin of the Arabian Shield, and were deposited in a passive margin setting after the stabilization of the Arabian Shield following the Oligocene Rifting Orogeny.

References

Abd el Hady MM (1988). Durability of monumental sandstone in Upper Egypt. In: Marinos PG, Koukis GC, editors. Engineering Geology of Ancient Works, Monuments and Historical Sites. Rotterdam, the Netherlands: A.A. Balkema, pp. 825–831.

Abd el Hady MM (2000). The deterioration of Nubian sandstone blocks in the Ptolemaic temples in Upper Egypt. In: Proceedings of the 9th International Congress on the Deterioration and Conservation of Stone, Venice, Italy. Amsterdam, the Netherlands: Elsevier, pp. 783–792.

Abu-Zeid MM, Amer KM, El-Mohammady RA (1989). Petrology, mineralogy and provenance of sandstones of "Nubia" facies in west central Sinai. Earth Sciences Series 3, Middle East Research Centre, Ain Shams University: 20–34.

Abu-Zeid, MM, Amer KM, Yanni NN, El-Wekeil SS (1991). Petrology, mineralogy and sedimentation of the Paleozoic sequence of Gabal Qattar, Wadi Feiran, Sinai, Egypt. J Geol 34: 145–169.

Ahmad I, Chandra R (2013). Geochemistry of loess-paleosol sediments of Kashmir Valley, India: provenance and weathering. J Asian Earth Sci 66: 73–89.

Al-Habri OA, Khan MM (2008). Provenance, diagenesis, tectonic setting and geochemistry of Tawil sandstone (Lower Devonian in central Saudi Arabia, J Asian Earth Sci 33: 278–287.

Amer KM, Abu-Zeid MM, El-Mohammady RA (1989). Particle-size distribution and depositional environment of the sandstones of "Nubia" facies in west central Sinai. Earth Sciences Series 3, Middle East Research Centre, Ain Shams University: 146–160.

Amireh BS (1991). Mineral composition of the Cambrian -Cretaceous Nubian series of Jordon: provenance, tectonic setting and climatological implication. Sediment Geo1 71: 99–119.

Armstrong-Altrin JS (2014) Evaluation of two multidimensional discrimination diagrams from beach and deep-sea sediments from the Gulf of Mexico and their application to Precambrian clastic sedimentary rocks. Int Geol Rev (in press).

Armstrong-Altrin JS, Lee YI, Kasper-Zubillaga, JJ, Carranza-Edwards A, Garcia D, Eby N, Balaram V, Cruz-Ortiz NL (2012). Geochemistry of beach sands along the Western Gulf of Mexico, Mexico: implication for provenance. Chem Erde Geochem 72: 345–362.

Armstrong-Altrin JS, Lee YI, Verma SP, Ramasamy S (2004). Geochemistry of sandstones from the Upper Miocene Kudankulam Formation, southern India: implications for provenance, weathering, and tectonic setting. J Sediment Res 74: 285–297.

Armstrong-Altrin JS, Machain-Castillo ML, Rosales-Hoz L, Carranza-Edwards A, Sanchez-Cabeza JA, Ruíz-Fernández AC (2015). Provenance and depositional history of continental slope sediments in the Southwestern Gulf of Mexico unraveled by geochemical analysis. Cont Shelf Res 95: 15–26.

Armstrong-Altrin JS, Nagarajan R, Lee YI, Kasper-Zubillaga JJ, Córdoba-Saldaña LP (2014) Geochemistry of sands along the San Nicolás and San Carlos beaches, Gulf of California, Mexico: implication for provenance. Turk J Earth Sci 23: 533–558.

Armstrong-Altrin JS, Nagarajan R, Madhavaraju J, Rosalez-Hoz L, Lee YI, Balaram V, Cruz-Martinez A, Avila-Ramirez G (2013). Geochemistry of the Jurassic and upper Cretaceous shales from the Molango Region, Hidalgo, Eastern Mexico: implications of source-area weathering, provenance, and tectonic setting. CR Geosci 345: 185–202.

Armstrong-Altrin JS, Verma SP (2005). Critical evaluation of six tectonic setting discrimination diagrams using geochemical data of Neogene sediments from known tectonic setting. Sediment Geol 177: 115–129.

Asiedu DK, Suzui S, Shibata T (2000). Provenance of sandstones from the Lower Cretaceous Sasayama Group, inner zone of southwest Japan. Sediment Geol 131: 9–24.

Aston BG, Harrell JA, Shaw I (2000). Stone. In: Nicholson PT, Shaw I, editors. Ancient Egyptian Materials and Technology. Cambridge, UK: Cambridge University Press, pp. 5–77.

Basu A, Young S, Suttner LJ, James WC, Mack CH (1975). Re-evaluation of the use of undulatory extinction and polycrystallinity in detrital quartz for provenance interpretation. J Sediment Petrol 45: 873–882.

Beitak M (1975). Die Identifizierung der Stadtanlage Tall el-Daba – Qantir mit. Auris und der Ramsesstadt, 2: 1–21 (in German).

Bhatia MR (1983). Plate tectonics and geochemical composition of sandstones. J Geol 91: 611–627.

Bhatia MR, Crook KAW (1986). Trace element characteristics of greywackes and tectonic setting discrimination of sedimentary basins. Contrib Mineral Petr 92: 181–193.

Blatt H, Middleton G, Murray R (1980). Origin of Sedimentary Rocks. 2nd ed. Englewood Cliffs, NJ, USA: Prentice Hall.

Carver RE (1971). Procedures in Sedimentary Petrology. New York, NY, USA: John Wiley.

Cox R, Lowe DR, Cullers RL (1995). The influence of sediment recycling and basement composition on evolution of mudrock chemistry in the southwestern United States. Geochim Cosmochim Ac 59: 2919–2940.

Cullers RL (1994). The controls on the major and trace element variation of shales, siltstones, and sandstones of Pennsylvanian-Permian age from uplifted continental blocks in Colorado to platform sediment in Kansas, USA. Geochim Cosmochim Ac 58: 4955–4972.

Cullers RL (2000). The geochemistry of shales, siltstones and sandstones of Pennsylvanian–Permian age, Colorado, U.S.A.: implications for provenance and metamorphic studies. Lithos 51: 181–203.

Cullers RL, Podkovyrov VN (2000). Geochemistry of the Mesoproterozoic Lakhanda shales in southeastern Yakutia, Russia: implications for mineralogical and provenance control, and recycling. Precambrian Res 104: 77–93.

Dabbagh ME, Rogers JJ (1983). Depositional environments and tectonic significance of the Wajid Sandstone of southern Saudi Arabia. J Afr Earth Sci: 47–57.

Dar MA (1998). Mineralogy and chemistry of the mangrove vegetation in Hurghada-Quseir area, Red Sea, Egypt. MSc, Suez Canal University, Ismailia, Egypt.

Dickinson WR (1970). Interpreting detrital modes of greywacke and arkose. J Sediment Petrol 40: 695–707.

Dickinson WR, Beard LS, Brakenridge GR, Erjavec JL, Ferguson RC, Inman KF, Knepp RA, Lindberg FA, Ryberg PT (1983). Provenance of North American Phanerozoic sandstones in relation to tectonic setting. J Geol Soc Amer 94: 222–235.

Dickinson WR, Suczek CA (1979). Plate tectonics and sandstone compositions. American Association of Petroleum Geologists 63: 2164–2182.

Dott RH (1964). Wackes, greywacke and matrix: what approach to immature sandstone classification. J Sediment Petrol 34: 625–632.

EAIS (2005). Egyptian Antiquities Information System Project. Geographical Information System, Cahiers of Sharqiya Governorate. Cairo, Egypt: Supreme Council of Antiquities.

Fedo CM, Nesbitt HW, Young GM (1995). Unraveling the effects of K metasomatism in sedimentary rocks and paleosols with implications for palaeoweathering conditions and provenance. J Geol 23: 921–924.

Folk RL (1966). A review of grain-size parameters. Sedimentology 6: 73–96.

Folk RL (1974). Petrology of Sedimentary Rocks. Austin, TX, USA: Hemphill Publications.

Friedman GM, Sander JE (1978). Principals of Sedimentology. New York, NY, USA: John Wiley.

Garver JI, Royce PR, Smick TA (1996). Chromium and nickel in shale of the Taconic Foreland: a case study for the provenance of fine-grained sediments with an ultramafic source. J Sediment Res 66: 100–106.

Gazzi P (1966). Le arenarie del fl ysch sopracretaceo dell'Appennino modensese: Correlazioni con il flysch di Monghidoro. Mineralogica et Petrographica Acta 12: 69–97 (in Italian).

Harrell JA (2002). Pharaonic stone quarries in the Egyptian deserts. In: Friedman R, editor. Egypt and Nubia – Gifts of the Desert. London, UK: British Museum Press, pp. 232–243.

Harrell JA, Madbouly MI (2006). An ancient quarry for siliceous sandstone at Wadi Abu Aggag, Egypt. Sahara 17: 51–58.

Heizer RF, Stross F, Hester TR, Albee A, Perlman J, Asaro F, Bowman H (1973). The colossi of Memnon revisited. Science 184: 1219–1225.

Heldal T, Bloxam EG, Storemyr P, Kelany A (2005). The geology and archaeology of the ancient silicified sandstone quarries at Gebel Gulab and Gebel Tingar, Aswan, Egypt. Marmora. International Journal of Archaeology, History and Archaeometry of Marbles and Stones 1: 11–35.

Hermina M, Klitzsch E, List FK (1989). Stratigraphic Lexicon and Explanatory Notes to the Geological Map of Egypt 1: 500.000. Cairo, Egypt: Conoco Inc.

Herron MM (1988). Geochemical classification of terrigenous sands and shales from core or log data. J Sediment Petrol 58: 820–829.

Hirst DM (1962). The geochemistry of modern sediments from the Gulf of Paria. II. The location and distribution of trace elements. Geochim Cosmochim Ac 26: 1174–1187.

Hofer G, Wagreich M, Neuhuber S (2013). Geochemistry of fine-grained sediments of the Upper Cretaceous to Paleogene Gosau Group (Austria, Slovakia): implications for paleoenvironmental and provenance studies. Geosci Front 4: 449–468.

Ingersoll RV, Bulard TF, Ford RL, Grimm JP, Pickle JP, Sares SW (1984). The effect of grain size on detrital modes: a test of the Gazzi-Dickinson point-counting method. J Sediment Petrol 54: 103–116.

Ingersoll RV, Suczek CA (1979). Petrology and provenance of Neogene sand from Nicobar and Bengal fans, DSDP sites 211 and 218. J Sediment Petrol 49: 1217–1228.

Jafarzadeh M, Harami RM, Amini A, Mahboubi A, Farzaneh F (2013). Geochemical constraints on the provenance of Oligocene-Miocene siliciclastic deposits (Zivah Formation) of NW Iran: implications for the tectonic evolution of the Caucasus. Arab J Geosci 7: 4245–4263.

Keller WD (1956). Clay minerals as influenced by environments of their formation. American Association of Petroleum Geologists 40: 2689–2710.

Khanchuk AI, Nevstruev VG, Berdnikov NV, Nechaev VP (2013). Petrochemical characteristics of carbonaceous shales in the eastern Bureya massif and their precious-metal mineralization. Russ Geol Geophys 54: 627–636.

Klemm DD, Klemm R (2001). The building stones of ancient Egypt – a gift of its geology. J Afr Earth Sci 33: 631–642.

Klemm DD, Klemm R (2008). Stone and Stone Quarries in Ancient Egypt. London, UK: British Museum Press.

Klemm DD, Klemm R, Steclaci L (1984). Die pharaonischen Steinbrüche des Silifizierten Sandsteins in Ägypten und die Herkunft der Memnon-Kolosse. Mitteilungen des Deutschen Archaologischen Instituts Abteilung Kairo 40: 207–220 (in German).

Klemm R, Klemm DD (1993). Steine und Steinbruche im alten Agypten. Berlin, Germany: Springer Verlag (in German).

Knox RWOB, Stadelmann R, Harrell JA, Heldal T, Sourouzian H (2009). Mineral fingerprinting of Egyptian siliceous sandstones and the quarry source of the Colossi of Memnon. In: Abu-Jaber N, Bloxam EG, Degryse P, Heldal T, editors. Quarry Scapes: Ancient Stone Quarry Landscapes in the Eastern Mediterranean. Oslo, Norway: Geological Survey of Norway Special Publication, pp. 77–85.

Kroonenberg SB (1994). Effects of provenance, sorting and weathering on the geochemistry of fluvial sands from different tectonic and climatic environments. In: Proceedings of the 29th International Geological Congress, Part A: 69–81.

Lonnie TP (1982). Mineralogic and chemical composition of marine and nonmarine transitional clay beds on south shore of Long Island, New York. J Sediment Petrol 52: 529–536.

Martinet G (1992). Grès et mortiers du temple d' Amon à Karnak (Haute Egypte). Etude des altérations, aide à la restauration. Paris, France: Laboratoire Central des Ponts et Chaussées.

McBride EF (1963). A classification of common sandstones. J Sediment Petrol 33: 664–669.

McLennan SM, Hemming S, McDaniel DK, Hanson GN, (1993). Geochemical approaches to sedimentation, provenance, and tectonics. In: Johnsson MJ, Basu A, editors. Processes Controlling the Composition of Clastic Sediments. Boulder, CO, USA: Geological Society of America Special Paper, pp. 21–40.

Morton AC (1985). Heavy minerals in provenance studies. In: Zuffa GG, editor. Provenance of Arenite. Dordrecht, the Netherlands: Reidel, pp. 249–277.

Nagarajan R, Armstrong-Altrin JS, Nagendra R, Madhavaraju J, Moutte J (2007). Petrography and geochemistry of terrigenous sedimentary rocks in the Neoproterozoic Rabanpalli Formation, Bhima Basin, Southern India: implications for paleoweathering conditions, provenance and source rock composition. J Geol Soc India 70: 297–312.

Nesbitt HW, Young GM (1982). Early Proterozoic climates and plate motions inferred from major element chemistry of lutites. Nature 299: 715–717.

Nowrouzi Z, Moussavi-Harami R, Mahboubi A, Gharaie MHM, Ghaemi F (2013). Petrography and geochemistry of Silurian Niur sandstones, Derenjal Mountains, East Central Iran: implications for tectonic setting, provenance and weathering. Arab J Geosci 7: 2793–2813.

Pettijohn FJ (1975). Sedimentary Rocks. 3rd ed. New York, NY, USA: Harper and Row.

Pettijohn FJ (1984). Sedimentary rocks. 3rd ed. New Delhi, India: India CBS Publ. and Dist.

Pettijohn FJ, Potter PE, Siever R (1987). Sand and Sandstone. New York, NY, USA: Springer.

Pittman ED (1970). Plagioclase as an indicator of provenance in sedimentary rocks. J Sediment Petrol 40: 591–598.

Potter PE (1978). Petrology and chemistry of modern Big River sands. J Geol 86: 423–449.

Roser BP, Korsch RJ (1986). Determination of tectonic setting of sandstone-mudstone suites using SiO₂ content and K₂O/Na₂O ratio. J Geol 94: 635–650.

Roser BP, Korsch RJ (1988). Provenance signatures of sandstone-mudstone suites determined using discrimination function analysis of major element data. Chem Geol 67: 119–39.

Said R (1990). The Geology of Egypt. Rotterdam, the Netherlands: A.A. Balkema.

Schwab FL (1975). Framework mineralogy and chemical composition of continental margin type sandstone. Geology 3: 487–490.

Shadan M, Hosseini-Barzi M (2013). Petrography and geochemistry of the Ab-e-Haji Formation in central Iran: implications for provenance and tectonic setting in the southern part of the Tabas block. Rev Mex Cien Geol 30: 80–95.

Stadelmann R (1984). Die Herkunft der Memnon-Kolosse: Heliopolis oder Aswan? Mitteilungen des Deutschen Archäologischen Instituts Abteilung Kairo 40: 291–296.

Suttner LJ, Basu A, Mack GH (1981). Climate and the origin of quartz arenites. J Sediment Petrol 51: 235–246.

Suttner LJ, Dutta PK (1986). Alluvial sandstone composition and paleoclimate, I. Framework mineralogy. J Sediment Petrol 56: 329–345.

Tao H, Wang Q, Yang X, Jiang L (2013). Provenance and tectonic setting of Late Carboniferous clastic rocks in west Junggar, Xinjiang, China: a case from the Hala-alat mountains. J Asian Earth Sci 64: 210–222.

Tawadros EE (2001). Geology of Egypt and Libya. Rotterdam, the Netherlands: A.A. Balkema.

Taylor SR, McLennan SM (1985). The Continental Crust: Its Composition and Evolution. Oxford, UK: Blackwell.

Tsuzuki Y, Kawabe I (1983). Polymorphic transformations of kaolin minerals in aqueous solutions. Geochim Cosmochim Ac 47: 59–66.

Turekian KK, Michael HC (1960). The geochemistries of chromium, cobalt and nickel. Int Geol Cong 1: 14–27.

Varille A (1933). L'inscription dorsale du colosse méridionale de Memnon. Annales du Service des Antiquites de l'Egypte 33: 85–94 (in French).

Vdačný M, Vozárová A, Vozár J (2013). Geochemistry of the Permian sandstones from the Malužiná Formation in the Malé Karpaty Mts (Hronic Unit, Western Carpathians, Slovakia): implications for source-area weathering, provenance and tectonic setting. Geol Carpath 64: 23–38.

Verma SP, Armstrong-Altrin JS (2013). New multi-dimensional diagrams for tectonic discrimination of siliciclastic sediments and their application to Precambrian basins. Chem Geol 355: 117–180.

Weltje GJ, Meijer XD, De Boer PL (1998). Stratigraphic inversion of siliciclastic basin fills: a note on the distinction between supply signals resulting from tectonic and climatic forcing: Basin Research 10: 129–153.

Young SW (1976). Petrographic textures of detrital polycrystalline quartz as an aid to interpreting crystalline source rocks. J Sediment Petrol 46: 595–603.

Zaid SM (2006). Geo-environmental assessment of east Nile Delta, Egypt. PhD, Zagazig University, Zagazig, Egypt.

Zaid SM (2012). Provenance, diagenesis, tectonic setting and geochemistry of Rudies sandstone (Lower Miocene), Warda Field, Gulf of Suez, Egypt. J Afr Earth Sci 66–67: 56–71.

Zaid SM (2013). Provenance, diagenesis, tectonic setting and reservoir quality of the sandstones of the Kareem Formation, Gulf of Suez, Egypt. J Afr Earth Sci 85: 31–52.

Zaid SM, Gahtani FA (2015). Provenance, diagenesis, tectonic setting and geochemistry of Hawkesbury sandstone (Middle Triassic), southern Sydney Basin, Australia. Turk J Earth Sci 24: 72–98.